JGR Solid Earth

RESEARCH ARTICLE
10.1029/2022JB025670

Special Section:
Advances in understanding volcanic processes

Lithium Isotope Constraints on Slab and Mantle Contribution to Arc Magmas

Wei Zhang[1], **Hiroshi Kitagawa**[1], **and Eizo Nakamura**[1]

[1]The Pheasant Memorial Laboratory for Geochemistry and Cosmochemistry, Institute for Planetary Materials, Okayama University, Tottori, Japan

Key Points:

- Volcanic rocks in the Chugoku district in Southwest Japan show large δ^7Li variation (−1.9‰ to +7.4‰)
- Li isotopes fractionate to the limited extent during arc magma production
- Slab-derived δ^7Li features can be preserved if slab-derived fluids/melts have distinct δ^7Li values from mantle and ascend rapidly

Supporting Information:

Supporting Information may be found in the online version of this article.

Correspondence to:

H. Kitagawa,
kitaga-h@cc.okayama-u.ac.jp

Citation:

Zhang, W., Kitagawa, H., & Nakamura, E. (2023). Lithium isotope constraints on slab and mantle contribution to arc magmas. *Journal of Geophysical Research: Solid Earth*, *128*, e2022JB025670. https://doi.org/10.1029/2022JB025670

Received 21 SEP 2022
Accepted 12 APR 2023

Author Contributions:

Conceptualization: Hiroshi Kitagawa, Eizo Nakamura
Formal analysis: Wei Zhang
Investigation: Wei Zhang, Hiroshi Kitagawa
Methodology: Wei Zhang
Project Administration: Hiroshi Kitagawa, Eizo Nakamura
Supervision: Eizo Nakamura
Visualization: Wei Zhang
Writing – original draft: Wei Zhang, Hiroshi Kitagawa
Writing – review & editing: Wei Zhang, Hiroshi Kitagawa, Eizo Nakamura

Abstract Dehydration of subducting oceanic lithosphere (slab) induces Li-isotope fractionation between the fluid and the slab, suggested by the δ^7Li variation (~10‰) in exhumed subduction complexes. Given that arc magmas represent melt of the supraslab mantle, a large δ^7Li variation is anticipated for arc volcanic rocks. However, the δ^7Li values in these rocks are mostly homogeneous within the range of mid-ocean ridge basalts (+1.6 to +5.6‰). The lack of a subduction-related δ^7Li signature has been explained by (a) homogenization by mixing of different magma sources, (b) loss of Li from the slab via dehydration, or (c) homogenization by diffusive exchange of slab-derived Li and the mantle. The Chugoku district in SW Japan is an ideal place to study the process responsible for Li-isotope variation in arc magmas, since the Chugoku volcanic rocks show large δ^7Li variation (−1.9 to +7.4‰). High δ^7Li values (+6.3 to +7.4‰) are found in some high-Sr andesites and dacites (adakites) whereas low δ^7Li values (−1.0 to −0.1‰) are found in high-Mg andesites. The parental magmas of these rocks have been sourced from subducted oceanic crust and sediments, respectively, with various extents of the interaction with wedge mantle. The limited extents of Li isotope modification are indicated by the similarity of the δ^7Li values of these rocks and their supposed sources. The models for a slab dehydration and a diffusive exchange between slab-derived melt and mantle demonstrate that the δ^7Li signatures of the sources can be preserved in the adakites if they ascent rapidly in mantle.

Plain Language Summary Many of Earth's volcanoes occur near the trenches, where one plate subducts beneath another. These volcanoes are formed as a result of the melting of mantle that contains materials of subducted plates and the transportation of melts through the mantle. A quantitative understanding of these important processes has been hampered by the lack of geochemical tools to examine consecutive chemical reactions beneath the volcanoes. Here we conducted a lithium isotope investigation of the volcanic rocks from the Chugoku district in Southwest Japan. This district hosts the volcanoes of andesites and dacites which have been derived from the melting of materials in the subducted plate. We found that these volcanic rocks preserve Li-isotope compositions of the original materials when they melted. This in turn suggests that these magmas ascent rapidly (<300,000 years) in the mantle.

1. Introduction

It is generally accepted that fluids play a critical role in the production of arc magmas (Ishikawa & Nakamura, 1994; Nakamura et al., 1985; Perfit et al., 1980; Sakuyama & Nesbitt, 1986). Fluids lower the solidi of magma sources, thus inducing melting without the need for mantle with an anomalously high temperature. Fluids are considered to be expelled from oceanic lithospheric rocks during their subduction beneath an arc. Fluids also transport elements via dissolution of materials in subducted oceanic lithosphere (slab), resulting in elemental enrichments in arc magmas. The extents of the enrichments are related to the elemental solubility of a given element of group. For example, alkali metals and alkaline earth metals are highly soluble in fluids and thus are enriched in arc magmas (Kessel et al., 2005).

Lithium represents an element with a high solubility in fluids (Kessel et al., 2005). It has two isotopes (^{7}Li and ^{6}Li) that fractionate during element partitioning between two substances; for example, fluid and rock or vapor and melt (Penniston-Dorland et al., 2017; Tomascak et al., 2016). In general, ^{7}Li is preferentially transferred into fluids (Caciagli et al., 2011; Wunder et al., 2006), and as a result, sub-arc mantle hydrated by fluids released by incipient dehydration of a slab would be enriched in ^{7}Li. Arc volcanic rocks, in particular those occurring in fore-arc region, are thus expected to record high δ^7Li values from their hydrated sources. However, δ^7Li values of most arc rocks fall within the range of unaltered mid-ocean ridge basalts (MORB with δ^7Li = +1.6 to

+5.6‰; H. R. Marschall et al., 2017; Tomascak et al., 2008). Given that MORB likely represent a well-averaged melt extracted from the upper mantle (Langmuir et al., 1992), the δ^7Li value of MORB well approximates the δ^7Li value of the upper mantle (+1.4 to +5.2‰), postulated by the analyses of pristine mantle rocks (Jeffcoate et al., 2007; Lai et al., 2015; Magna, Wiechert, & Halliday, 2006; Pogge von Strandmann et al., 2011; Seitz et al., 2004). Accordingly, the similarity of δ^7Li between MORB and arc volcanic rocks has been interpreted to reflect the prevalence of the upper mantle as a source of Li in arc magmas (Tomascak et al., 2002). The apparent similarity in δ^7Li values of arc magmas and MORB has been explained by the three scenarios: (a) homogenization by mixing of different magma sources, (b) loss of Li from the slab via dehydration, or (c) homogenization by diffusive exchange of slab-derived Li and the mantle.

Scenario 1 explains the apparent similarity in δ^7Li values of arc magmas and MORB by the contributions of Li from various materials of the subducting oceanic lithosphere, including sediments (silicate/carbonate), basalts and serpentinites. Sediments have high [Li] (>10 $\mu g \cdot g^{-1}$ except for specific types such as foram ooze, marl and diatom, or volcano clastics; Bouman et al., 2004; Brens et al., 2019; Chan et al., 2006; Plank, 2014; Tang et al., 2014; You et al., 1995), hence fluids or melts from sediments could represent a significant Li budget in arc magma sources. Some serpentinized abyssal peridotites have δ^7Li values as high as +20‰ (Brant et al., 2012; Decitre et al., 2002; Vils et al., 2008), and hence could be another potential ^{7}Li-enriched reservoir. Previous studies found that δ^7Li values of sediments subducting in some trenches ($+3.9 \pm 2.3$‰ [1σ]; Plank, 2014; Tang et al., 2014) are similar to that of the mantle (i.e., δ^7Li of MORB, +1.6 to +5.6‰). Thus, if sediment dominates subduction Li inputs, the arc magmas should have δ^7Li values indistinguishable from MORB.

Scenario 2 explains the apparent similarity in δ^7Li values of arc magmas and MORB by extensive dehydration of the oceanic lithosphere (Leeman et al., 2004; Magna, Wiechert, Grove, et al., 2006; Moriguti et al., 2004). The dehydration was proposed to substantially lower [Li] and δ^7Li values before the slab reaches the depth (70–170 km; Syracuse & Abers, 2006) beneath arc volcanoes (Moriguti & Nakamura, 1998; Zack et al., 2003). In particular, dehydration occurs at shallower depths in relatively warm subduction zones (Abers et al., 2017). Accordingly, the sources of magmas in warm subduction zones are considered to contain little slab-derived Li. Instead, the Li in the magma source is dominated by that from the mantle, which should have a δ^7Li value similar to MORB. This inference is consistent with across-arc variations in [Li] and δ^7Li value of some arc lavas which include low-[Li] rocks with MORB-like δ^7Li value from back-arc regions (e.g., central America; Tomascak et al., 2000).

Scenario 3 explains the apparent similarity in δ^7Li values of arc magmas and MORB by re-equilibration of Li between slab-derived fluids and the overlying mantle. When fluids ascend through the mantle, they should react with the mantle. The abundance of Li in the mantle ($\sim$1 $\mu g \cdot g^{-1}$; H. R. Marschall et al., 2017) appears to be high enough to alter Li isotope composition of fluids to be similar to that of the mantle (Caciagli et al., 2011; Halama et al., 2009; Magna, Wiechert, Grove, et al., 2006; Parkinson et al., 2007; Tomascak et al., 2000, 2002).

In this study, Li isotopic compositions of the late Cenozoic volcanic rocks from the Chugoku district in Southwest (SW) Japan arc are investigated. This district hosts various types of volcanic rocks which represent melts derived from subducted sediments (high-Mg andesite; Shimoda et al., 1998) and oceanic crust (high-Sr andesites and dacite [adakite]; Feineman et al., 2013; Pineda-Velasco et al., 2018). We find that these rocks show δ^7Li values beyond the range of MORB, probably due to contributions from subducted sediments and oceanic crust. This in turn allows us to examine the role of slab contribution in Li isotopic systematics of the arc. We also investigate Li-isotope analyses of other types of volcanic rocks (basalts) and integrate Sr-Nd-Hf-Pb isotope analyses in order to examine the role of slab-mantle interaction in the Li isotopic systematics of the arc.

2. Geological Setting and Samples

Southwest Japan is located close to the convergent plate margin where the Philippine Sea (PHS) plate is subducting beneath the Eurasian plate via the Nankai Trough (Figure 1a). The Nankai Trough is a shallow trench, owing to subduction of the young plate in the depression (Shikoku Basin) and accumulation of sediments (>1,000-m thickness; Moore et al., 2001). The latter factor also relates to the development of an accretionary complex at the edge of the overlying Eurasian Plate. The surface exposure of this complex is dominated by metamorphosed sedimentary rocks found in the onshore areas in Shikoku, Kyushu and Honshu, termed the Shimanto Belt (Taira et al., 1988).

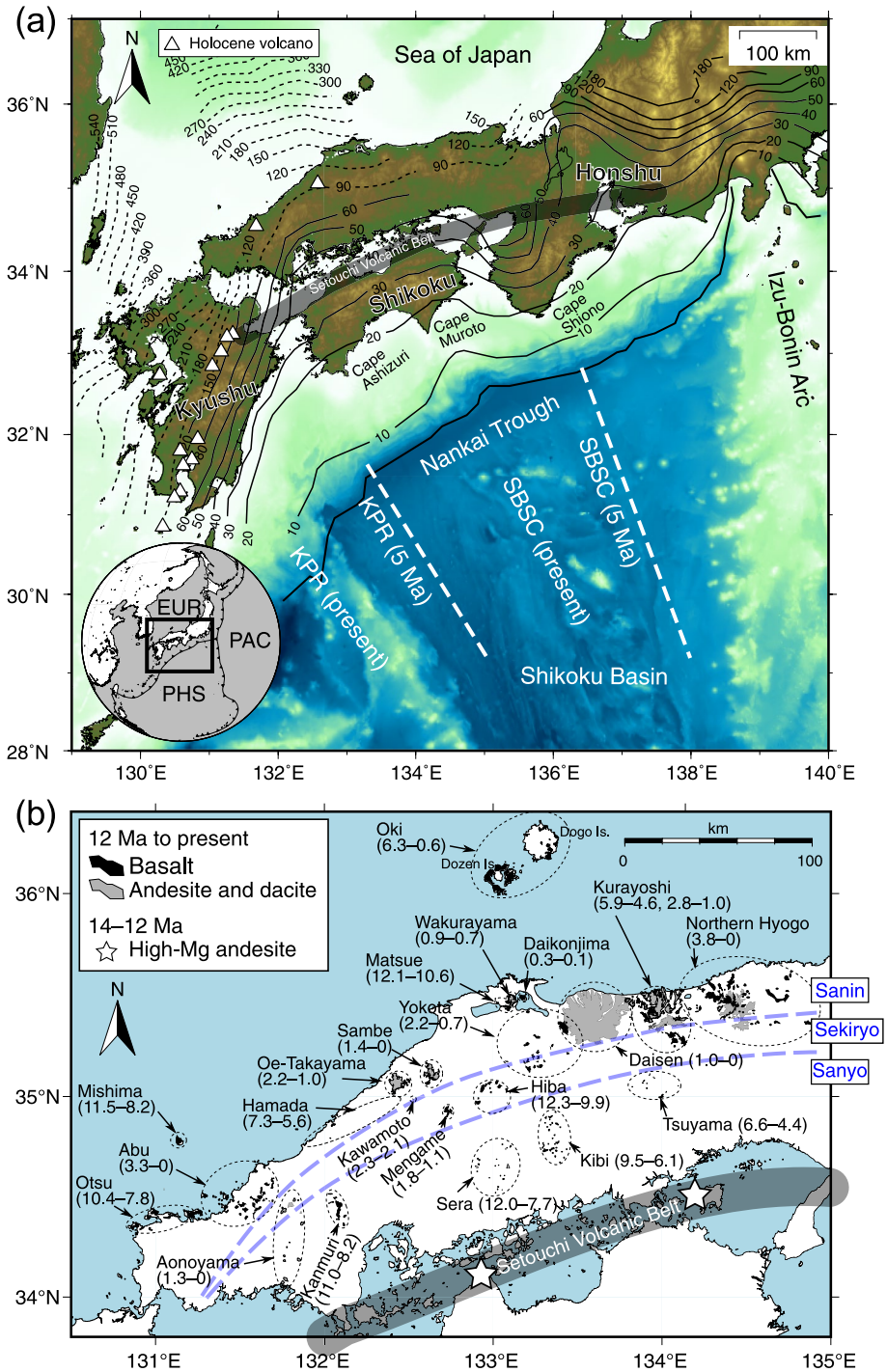

Figure 1. (a) Map of SW Japan including the Chugoku district. Depth (km) of the top of the subducting slab is shown with solid (seismic slab) and dotted (aseismic slab) lines (Asamori & Zhao, 2015). SBSC, Shikoku Basin Spreading Center (extinct); KPR, Kyushu-Palau Ridge (Mahony et al., 2011). White triangles mark the locations of Holocene volcanoes in western Honshu (Chugoku) and Kyushu (Japan Meteorological Agency, 2013). An insert map shows plate configuration around Japan (PHS, Philippine Sea plate; PAC, Pacific plate; EUR, Eurasian plate). (b) Locations of volcanic fields in the Chugoku district (age [Ma] in parenthesis). White stars mark the localities of high magnesium andesites in the Setouchi Volcanic Belt (Tatsumi & Hanyu, 2003). Blue broken lines denote the borders of the trench-parallel zones (Sanyo, Sekiryo and Sanin) after Iwamori (1991).

The Shikoku Basin plate has complex surface morphology (Figure 1a), owing to the topographic prominence (Izu-Bonin Arc, Kinan Seamounts, and Kyushu-Palau Ridge) within or in periphery of the Shikoku Basin. Seismic tomography reveals that the PHS slab is subducting at a shallow angle (~30°) up to 80- to 100-km depth (Asamori & Zhao, 2015). Above the shallowly subducting slab, a series of Quaternary volcanoes are distributed along the northern coast to the west of the Chugoku district (Figure 1a). Beneath northern coastal region in the Chugoku district, the subduction angle abruptly changes to be steeper (~60°) till 500 km depth. This feature is interpreted as a result of the impingement of hot and buoyant mantle on the base of the PHS slab (Nguyen et al., 2020). Another feature of the PHS slab is the presence of aseismic discontinuities beneath the northern coastal region in this district, interpreted as slab tears (Zhao et al., 2012).

The volcanism in the Chugoku district occurred during the last 12 Myrs, which was preceded by volcanism in the south of the Chugoku district termed the Setouchi Volcanic Belt (SVB, Figure 1b) that occurred 14–12 million years ago (Ma). The volcanism in the SVB is dominated by eruptions of basalts and high magnesium andesites (Shimoda et al., 1998; Tatsumi & Hanyu, 2003). The volcanism in the Chugoku district mainly produced basalts that formed clusters of monogenetic volcanoes (10–50 km in diameter) (Figure 1b; Iwamori, 1991; Kimura et al., 2005). Nguyen et al. (2020) recognized 22 discrete volcanic fields (see Figure 1b) and divided their activities after 12 Ma into three episodes; Episode 1 (12–8 Ma), Episode 2 (8–4 Ma), and Episode 3 (4 Ma to present). Volcanic rocks produced in these episodes occur in various places in the entire Chugoku district (Figure 1b). We follow this age division of the Chugoku volcanism. In Episode 3, voluminous eruptions of adakites occurred in the northern coastal regions in central Chugoku (Kurayoshi, Daisen, Sambe and Oe-Takayama) and the inland area in western Chugoku (Aonoyama). The eruptions occurred in the regions 80–100 km above the edges of the slab tears (Pineda-Velasco et al., 2018). Hereafter, the SVB and Chugoku regions are collectively referred to as the Chugoku district.

The samples used in this study are the volcanic rocks (14 Ma to recent) from the Chugoku district, collected by Feineman et al. (2013), Nguyen et al. (2020), and Pineda-Velasco et al. (2018). The basalts, andesites, and dacites in the sample collection are classified as part of either sub-alkaline or alkaline series. Also included in this study are the volcanic rocks from the SVB; those are TG1, SD-264 and JA-2. The former two samples were collected by Tatsumi and Ishizaka (1982a), whereas the latter one was collected by Geological Survey of Japan as a geochemical reference sample (Imai et al., 1995). These three samples have been used in geochemical studies of SVB volcanism, as they represent magmas erupted in different locations within SVB (Hanyu et al., 2002; Shimoda et al., 1998). We follow the trace-element-based nomenclature of these volcanic rocks following the previous studies (Kimura et al., 2014; Nguyen et al., 2020; Pineda-Velasco et al., 2018; Tatsumi & Ishizaka, 1982a); HMA (high magnesium andesite), OIB (ocean-island basalt), IAB (island-arc basalt), IAA (island-arc andesite), and ADK (adakite, i.e., high-Sr andesite and dacite). The classification for basalts is based on the extent of Nb and Ta depletions (Kimura et al., 2005, 2014; Nguyen et al., 2020); IAB shows marked depletions of Nb and Ta in trace-element abundance patterns, while OIB does not exhibit such an anomaly. The basaltic samples (IAB and OIB) selected for this investigation are less differentiated; the $Mg^{\#}$ values ($\equiv 100 \times Mg/(Mg + Fe^{2+})$ in molar) are 50–74 for IAB and 44–74 for OIB (where Fe^{2+}/Fe_{total} in molar is assumed to be 0.85). The HMA are primitive andesitic rocks with FeO*/MgO ratios <1 (where FeO* is total Fe as FeO) or $Mg^{\#} > 70$ (where Fe^{2+}/Fe_{total} in molar is assumed to be 0.85). The classification for andesites and dacites is based on the extent of Sr enrichment and Y depletion; ADK shows marked enrichment of Sr and depletion of Y (hence high Sr/Y ratio), while IAA does not exhibit such an anomaly. ADK samples do not include primitive rocks; $Mg^{\#}$ values of this type of rocks used in this study are 25–67 (where Fe^{2+}/Fe_{total} in molar is assumed to be 0.80). IAA samples are not included in this study. Major- and trace-element compositions of the studied samples are given in Table S1 in Supporting Information S1.

3. Analytical Methods

All the analyses in this study (isotope analyses of Li, Sr, Nd and Hf) were conducted at the Pheasant Memorial Laboratory for Geochemistry and Cosmochemistry, Institute for Planetary Materials, Okayama University at Misasa (Nakamura et al., 2003). Major and trace element compositions of these samples and Sr-Nd-Hf-Pb isotope compositions for most of them are reported in the literature (Feineman et al., 2013; Ishikawa & Nakamura, 1994; Ishizaka & Carlson, 1983; Moriguti & Nakamura, 1998; Nguyen et al., 2020; Pineda-Velasco et al., 2018) or obtained in this study (see Table S1 in Supporting Information S1).

Lithium isotopic compositions ($^{7}Li/^{6}Li$) were analyzed for 3 HMA, 17 IAB, and 25 ADK. Details about the sample dissolution, column chemistry, and mass spectrometric settings were reported in Zhang et al. (2022). Isotopic measurements were performed by a Thermo Fisher Neptune plus inductively coupled plasma mass spectrometer (ICP-MS) in static multicollection mode. Instrumental mass bias and drift were corrected by bracketed analyses of the standard (L-SVEC). The Li isotope composition of a given sample is reported in a $\delta^{7}Li$ notation ($\delta^{7}Li = \{(^{7}Li/^{6}Li)_{sample}/(^{7}Li/^{6}Li)_{L\text{-}SVEC} - 1\} \times 10^{3}$).

The $^{176}Hf/^{177}Hf$ ratios were determined for 2 HMA, 27 OIB, 31 IAB, and 29 ADK samples from the Chugoku district (total 89 samples). For 25 (10 IAB and 15 ADK) of the 89 samples for Hf isotope analysis, the $^{87}Sr/^{86}Sr$ and $^{143}Nd/^{144}Nd$ ratios were also determined as these data are not provided in Feineman et al. (2013) or Nguyen et al. (2020). Details about the procedures of sample dissolution, column chemistry, analytical method, and data correction are shown in Text S1 in Supporting Information S1.

4. Results

New $^{7}Li/^{6}Li$, $^{87}Sr/^{86}Sr$, $^{143}Nd/^{144}Nd$ and $^{176}Hf/^{177}Hf$ data for the selected samples of volcanic rocks from the Chugoku district are reported in Table 1. The $\delta^{7}Li$ values of the Chugoku volcanic rocks range from −1.9‰ to +7.4‰. The observed $\delta^{7}Li$ variation is far larger than the range found in unaltered MORB (+1.6‰ to +5.6‰; H. R. Marschall et al., 2017; Tomascak et al., 2008) and that of most other arcs (Figure 2). HMA in the Setouchi district shows a lower-than-MORB $\delta^{7}Li$ signature with smaller variation (−1.0 to −0.1‰, this study), compared with IAB and ADK in the Chugoku district (Figure 2). The $\delta^{7}Li$ values of most IAB show a variation as small as 2‰ ($\delta^{7}Li$ = +1.5 to +3.6‰) and fall within the range of MORB. Accordingly, the $\delta^{7}Li$ values of IAB do not show a clear temporal variation (Figure S5 in Supporting Information S1). Three IAB samples have $\delta^{7}Li$ values outside the range of MORB. Among these samples, the sample MAT-04 (Matsue), erupted in Episode 1, has a $\delta^{7}Li$ value (+6.29‰) higher than $\delta^{7}Li$ values of unaltered MORB, whereas KUR-17 (Kurayoshi), erupted in Episode 2, has a $\delta^{7}Li$ value (−1.95‰) lower than $\delta^{7}Li$ values of unaltered MORB. The second lowest $\delta^{7}Li$ value (−1.02‰) among IAB is found in an ultrapotassic lamprophyre, SER-11 (Sera), erupted in Episode 1, whereas the second highest $\delta^{7}Li$ value (+5.02‰) is found in an ultrapotassic lamprophyre, KAW-03 (Kawamoto), erupted in Episode 3. These lamprophyres also have Sr, Nd, or Hf isotopic compositions which define the lowest or highest values among IAB or are close to these extreme values. SER-11 has the highest $(^{87}Sr/^{86}Sr)_t$ (subscript t denotes age-corrected composition), the lowest $(^{143}Nd/^{144}Nd)_t$, and the second lowest $(^{176}Hf/^{177}Hf)_t$ among IAB, whereas KAW-03 has the third highest $(^{87}Sr/^{86}Sr)_t$, the second lowest $(^{143}Nd/^{144}Nd)_t$, and the lowest $(^{176}Hf/^{177}Hf)_t$ among IAB (Figure 3).

The $\delta^{7}Li$ values of ADK ($\delta^{7}Li$ = +1.2 to +7.4‰) largely overlap with those of IAB, and some ADK have $\delta^{7}Li$ values (+6.3‰ to +7.4‰) significantly higher than $\delta^{7}Li$ values of unaltered MORB. Such ADK are from the volcanic fields in the central Chugoku district, consisting of Wakurayama and Daisen. The eruption ages of the high-$\delta^{7}Li$ Daisen samples are older (0.4–0.5 Ma) than those of the other Daisen samples (<0.4 Ma) (Feineman et al., 2013). No samples with $\delta^{7}Li$ values lower than MORB were found among the ADK samples, when the analytical uncertainty was taken into consideration.

The $(^{176}Hf/^{177}Hf)_t$ of IAB and ADK, analyzed by this study, show variations of 0.28276–0.28310 and 0.28291–0.28310, respectively. The $(^{176}Hf/^{177}Hf)_t$ of 0.282876 and 0.282981 are given by Hanyu et al. (2002) for the HMA samples used for Li-isotope analysis in this study (Note that the values of $(^{176}Hf/^{177}Hf)_t$ used in this study are slightly different from those shown in Hanyu et al. (2002), resulted from re-normalization using the different values of the reference standard material [JMC 475]; see Text S1 in Supporting Information S1). The Aonoyama ADK and the Abu IAB possess higher $(^{176}Hf/^{177}Hf)_t$ than the other ADK and IAB, respectively. We also analyzed the $^{176}Hf/^{177}Hf$ ratios of the other type of basalts, namely OIB (see Section 2 for the classification), which show a range of $^{176}Hf/^{177}Hf$ ratio from 0.28277 to 0.28299. The observed variations in $^{176}Hf/^{177}Hf$ of the volcanic rocks in Abu (OIB and IAB), Aonoyama (ADK), Yokota (IAB), Daisen (ADK), Kurayoshi (OIB, IAB and ADK) and Northern Hyogo (OIB and IAB) in Episode 3 are essentially consistent with the data presented in Kimura et al. (2014) for the rocks from the same volcanic fields.

5. Discussion

Volcanic rocks from the Chugoku district in SW Japan show a significant variation in $\delta^{7}Li$ (−1.9 to +7.4‰), far beyond the $\delta^{7}Li$ range found in unaltered MORB. The overall $\delta^{7}Li$ variation is the largest among the

Journal of Geophysical Research: Solid Earth
10.1029/2022JB025670

Table 1
Li, Hf, Sr, Nd and Pb Isotopic Compositions of Late Cenozoic Volcanic Rocks From the Chugoku District, SW Japan

Sample name	Region	Latitude (°N)	Longitude (°E)	Age (Ma)	Episode[a]	$(^{176}Hf/^{177}Hf)_t$	$(^{143}Nd/^{144}Nd)_t$	$(^{87}Sr/^{86}Sr)_t$	$(^{206}Pb/^{204}Pb)_t$	$(^{207}Pb/^{204}Pb)_t$	$(^{208}Pb/^{204}Pb)_t$	Li (μg·g^{-1})	δ^7Li	MgO (wt%)	LOI (wt%)	FeO[b]/MgO	Mg#[c]	CIA[d]	Cs/Rb	Li/Y
IAB type																				
OTS-01	Otsu	34.348	130.839	9.10	1	**0.282834**	0.512628	0.705305	18.391	15.607	38.618	12.9		6.88	1.31	1.43	59.5	53	0.0148	0.72
OTS-05	Otsu	34.343	130.950	8.29	1	**0.282877**	**0.512612**	**0.705271**	18.377	15.602	38.595	9.41	**+3.14**	6.91	0.24	1.13	65.0	59	0.0081	0.48
OTS-06	Otsu	34.392	130.938	9.31	1	**0.282860**	0.512644	0.705159	18.382	15.609	38.606	12.7	**+2.84**	7.84	0.63	1.37	60.5	54	0.0159	0.86
OTS-10	Otsu	34.405	131.129	9.25	1	**0.282896**	**0.512675**	**0.704882**	18.279	15.587	38.472	8.50		10.21	1.38	0.81	72.0	61	0.0162	0.53
SER-11	Sera	34.851	132.834	12.0	1	**0.282821**	**0.512493**	**0.706591**				77.3	**−1.02**	6.67	1.94	1.14	64.8	49	0.0871	1.94
HIB-01	Hiba	34.991	132.900	10	1	**0.282905**			18.335	15.593	38.531	7.62		6.88	0.45	1.07	66.2	59	0.0083	0.37
HIB-04	Hiba	35.059	133.035	10.4	1	**0.282881**	**0.512605**	**0.705097**	18.357	15.593	38.557	10.5	**+3.41**	6.56	0.47	1.02	67.2	55	0.0057	0.62
HIB-06	Hiba	35.045	133.074	9.90	1	**0.282874**	**0.512609**	**0.705005**	18.338	15.589	38.540	7.45		6.73	0.81	1.08	65.9	62	0.0138	0.41
HIB-07	Hiba	34.987	133.077	10.1	1	**0.282883**	0.512614	0.704768	18.331	15.588	38.543	7.21	**+3.51**	8.31	0.19	0.93	69.3	58	0.0086	0.36
MAT-04	Matsue	35.452	133.069	11.0	1	**0.282984**	0.512667	0.704509	18.258	15.576	38.422	8.53	**+6.29**	7.27	1.81	1.00	67.7	55	0.0134	0.38
MKM-01	Kurayoshi (old)	35.494	134.102	5.03	2	**0.282900**	0.512665	0.705568	18.331	15.586	38.579	7.48	**+2.06**	5.07	−0.09	1.67	55.7	61	0.0350	0.40
KUR-16	Kurayoshi (old)	35.442	133.863	5	2	**0.282861**	**0.512617**	**0.705760**				7.17		8.23	1.19	1.01	67.6	61	0.0140	0.47
KUR-17	Kurayoshi (old)	35.443	133.859	5.15	2	**0.282873**	0.512621	0.705671	18.351	15.594	38.614	8.12	**−1.95**	7.11	0.50	1.23	63.0	59	0.0184	0.50
KRW-02	Kurayoshi (old)	35.258	134.100	4.99	2	**0.282859**	0.512587	0.705310	18.329	15.578	38.633	4.86	**+2.59**	8.35	0.97	1.21	63.5	64	0.0176	0.24
KRW-03	Kurayoshi (old)	35.256	134.138	5.43	2	**0.282894**	**0.512670**	**0.705356**	18.311	15.578	38.580	5.56		7.55	0.77	1.21	63.4	62	0.0082	0.33
KAW-03	Kawamoto	34.993	132.514	2.26	3	**0.282787**	**0.512528**	**0.705861**				18.6	**+5.02**	4.68	1.60	1.47	58.8	50	0.0129	0.99
MEN-02	Mengame	34.938	132.724	1.11	3	**0.282897**	0.512673	0.704906	18.310	15.581	38.523	9.80	**+1.45**	9.71	0.38	0.77	73.2	57	0.0086	0.33
ABU-06	Abu	34.442	131.498	1.57	3	**0.282876**	0.512626	0.705215	18.356	15.590	38.600	10.0		6.05	0.11	2.13	49.6	51	0.0384	0.53
ABU-11	Abu	34.479	131.444	0.06	3	**0.283009**	0.512839	0.703502	18.213	15.537	38.336	9.87	**+2.46**	7.51	0.46	1.16	64.3	59	0.0396	0.54
ABU-17	Abu	34.477	131.605	0.39	3	**0.282893**	0.512732	0.704504	18.254	15.553	38.451	10.6		7.49	−0.19	1.17	64.3	55	0.0054	0.56
ABU-21	Abu	34.487	131.625	0.18	3	**0.283091**	**0.512907**	**0.703546**				9.59	**+1.78**	8.30	−0.38	0.93	69.2	55	0.0100	0.57
ABU-23	Abu	34.493	131.645	0.18	3	**0.283097**	0.512913	0.703562	18.036	15.512	38.052	10.1	**+1.62**	7.91	0.86	0.96	68.5	55	0.0200	0.62
ABU-26	Abu	34.603	131.688	2.01	3	**0.282863**	0.512613	0.704858	18.359	15.603	38.614	12.0		4.39	0.16	1.76	54.4	52	0.0105	0.81
MAT-02	Yokota	35.418	133.185	1.2	3	**0.282960**	0.512743	0.704882	18.244	15.564	38.425	8.85		7.18	2.69	0.95	68.8	63	0.0143	0.50
YOK-01	Yokota	35.191	133.086	1.1	3	**0.282917**	0.512686	0.705458	18.308	15.580	38.517	7.84		7.48	0.19	0.84	71.5	56	0.0074	0.54
YOK-05	Yokota	35.160	133.209	1.32	3	**0.282947**	0.512697	0.705512	18.313	15.582	38.519	8.09	**+3.62**	9.47	0.48	0.72	74.3	59	0.0202	0.59
US-01	Kurayoshi (young)	35.452	133.919	1.00	3	**0.282755**	0.512476	0.706789	18.310	15.578	38.544	9.71		4.69	−0.17	1.65	56.0	59	0.0165	0.78
OGI-03	N. Hyogo	35.479	134.420	0.98	3	**0.282811**	0.512559	0.706422	18.358	15.593	38.621	13.2		4.29	0.84	1.74	54.6	57	0.0202	0.80
INA-01	N. Hyogo	35.500	134.299	2.74	3	**0.282875**	0.512584	0.706099	18.367	15.599	38.627	9.41	**+1.65**	5.17	0.63	1.75	54.5	59	0.0177	0.50
HYO-03	N. Hyogo	35.491	134.530	1.62	3	**0.282870**	0.512606	0.706028	18.321	15.586	38.586	8.73		5.29	0.26	1.38	60.4	56	0.0097	0.42
HYO-15	N. Hyogo	35.592	134.811	1.81	3	**0.282834**	**0.512683**	**0.703953**	18.202	15.556	38.408	11.0	**+2.06**	7.46	6.15	1.46	58.9	79	0.0043	0.36
ADK type																				
AON-03	Aonoyama	34.493	131.815	0.29	3		**0.512851**	**0.703442**	18.170	15.533	38.241	13.2		2.36	1.20	1.44	60.7	53	0.0185	1.51

Journal of Geophysical Research: Solid Earth
10.1029/2022JB025670

Table 1
Continued

Sample name	Region	Latitude (°N)	Longitude (°E)	Age (Ma)	Episode[a]	$(^{176}Hf/^{177}Hf)_t$	$(^{143}Nd/^{144}Nd)_t$	$(^{87}Sr/^{86}Sr)_t$	$(^{206}Pb/^{204}Pb)_t$	$(^{207}Pb/^{204}Pb)_t$	$(^{208}Pb/^{204}Pb)_t$	Li (μg·g^{-1})	δ^7Li	MgO (wt%)	LOI (wt%)	FeO[b]/MgO	Mg#[c]	CIA[d]	Cs/Rb	Li/Y
AON-04	Aonoyama	34.473	131.800	0.09	3	**0.283086**	**0.512845**	**0.703460**	18.146	15.527	38.200	11.7	**+3.26**	2.13	0.45	1.63	57.8	53	0.0173	1.14
AON-09	Aonoyama	34.448	131.765	0.30	3	**0.283028**	**0.512899**	**0.703562**	18.190	15.534	38.266	13.4	**+3.04**	2.20	0.53	1.53	59.2	52	0.0231	1.05
AON-17	Aonoyama	34.076	131.751	0.3	3	**0.283038**	**0.512888**	**0.703550**	18.123	15.532	38.225	19.0	**+3.06**	3.21	2.07	1.12	66.6	51	0.0371	2.09
AON-21	Aonoyama	34.254	131.774	0.38	3	**0.283102**	**0.512900**	**0.703545**	18.059	15.507	38.086	11.8	**+1.60**	2.89	1.03	1.55	59.1	52	0.0203	0.87
AON-22	Aonoyama	34.188	131.764	0.5	3	**0.283084**	**0.512924**	**0.703481**	18.083	15.521	38.140	15.3	**+2.44**	3.32	1.29	1.48	60.1	52	0.0304	0.77
OE-01	Oe-Takayama	35.070	132.427	1.52	3	**0.282948**	**0.512675**	**0.705015**	18.309	15.584	38.510	10.4		1.01	0.51	2.94	43.2	51	0.0346	1.44
OE-02	Oe-Takayama	35.090	132.435	1.5	3		**0.512662**	**0.705236**	18.328	15.590	38.538	12.4		0.36	1.00	6.82	24.6	52	0.0293	2.49
OE-03	Oe-Takayama	35.089	132.436	1.70	3	**0.282921**	**0.512665**	**0.705236**	18.327	15.589	38.536	14.7	**+3.42**	0.77	0.75	3.47	39.1	51	0.0403	2.30
OE-09	Oe-Takayama	35.115	132.409	1.05	3	**0.282983**	**0.512666**	**0.705040**	18.209	15.555	38.388	10.2	**+5.20**	1.49	0.39	1.88	54.3	50	0.0428	2.08
OE-10	Oe-Takayama	35.102	132.413	1.87	3	**0.282933**	**0.512719**	**0.704677**	18.284	15.580	38.484	14.6	**+5.64**	0.49	1.23	4.47	33.3	52	0.0477	2.71
OE-11	Oe-Takayama	35.107	132.424	1.83	3	**0.282913**	**0.512648**	**0.705284**	18.337	15.595	38.556	18.6	**+5.19**	1.08	2.00	2.38	48.4	51	0.0276	3.96
SAM-01[e]	Sambe	35.162	132.616	1.36	3	**0.283012**	0.512743	0.704832	18.234	15.550	38.370	10.1		1.78	1.20	2.33	48.9	57	0.0055	1.11
SAM-06	Sambe	35.135	132.631	0.07	3	**0.282995**	0.512737	0.704832	18.293	15.571	38.484	11.7		1.94	0.23	1.80	55.3	52	0.0463	1.74
SAM-14	Sambe	35.129	132.620	0.43	3	**0.282972**	0.512706	0.704957	18.299	15.576	38.504	16.3	**+2.40**	1.90	0.26	1.76	55.9	52	0.0554	2.47
SAM-16	Sambe	35.135	132.620	0.3	3	**0.282982**	0.512719	0.704832	18.288	15.566	38.469	16.0	**+2.46**	1.97	0.47	1.80	55.3	52	0.0488	2.21
SAM-20	Sambe	35.154	132.626	0.22	3	**0.282988**	0.512733	0.704738	18.293	15.572	38.484	12.5	**+3.00**	1.92	0.21	1.85	54.7	52	0.0450	1.80
SAM-21	Sambe	35.114	132.631	0.2	3	**0.282975**	0.512712	0.705057	18.305	15.575	38.493	13.9	**+4.93**	1.79	0.36	1.67	57.1	51	0.0616	2.07
WAK-01	Wakurayama	35.467	133.108	0.86	3	**0.283021**	**0.512747**	**0.704807**	18.275	15.569	38.444	8.10	**+7.44**	2.05	0.19	1.77	55.7	54	0.0222	1.34
WAK-02	Wakurayama	35.485	133.121	0.72	3	**0.283047**	**0.512800**	**0.704552**	18.245	15.558	38.391	10.5	**+7.12**	2.28	0.23	1.63	57.8	52	0.0250	1.66
WAK-03	Wakurayama	35.492	133.116	0.73	3	**0.283053**	**0.512768**	**0.704620**	18.253	15.561	38.403	10.3	**+6.35**	1.74	0.78	2.16	50.8	54	0.0229	1.63
2060707	Daisen	35.364	133.538	0.02	3	**0.282972**	0.512725	0.705097	18.314	15.579	38.514	13.8		1.80	0.07	2.02	52.5	51	0.0533	1.69
3052002	Daisen	35.355	133.555	0.06	3	**0.282982**	0.512713	0.704969	18.311	15.578	38.508	14.5	**+1.21**	1.84	0.38	2.05	52.1	51	0.0570	1.76
3053003	Daisen	35.328	133.566	0.51	3	**0.283009**	0.512703	0.705004	18.299	15.578	38.502	10.0	**+7.22**	2.11	0.73	1.85	54.7	53	0.0159	1.23
3060102	Daisen	35.355	133.507	0.46	3	**0.282993**	0.512707	0.705013	18.288	15.575	38.470	11.0	**+7.32**	1.90	0.32	2.12	51.3	54	0.0233	1.27
3060604	Daisen	35.403	133.589	0.41	3	**0.282993**	0.512714	0.705005	18.293	15.575	38.482	11.9	**+7.03**	2.00	0.42	1.90	54.0	53	0.0184	1.30
SAN2	Daisen	35.377	133.572	0.05	3	**0.283002**	0.512749	0.704676	18.291	15.574	38.482	11.3	**+4.66**	2.05	0.47	1.76	55.9	51	0.0323	1.35
YOK-11	Daisen	35.360	133.485	0.55	3	**0.283030**	0.512746	0.705065	18.286	15.573	38.465	12.3	**+4.88**	1.92	0.37	2.24	49.8	54	0.0377	1.55
TG-01	Kurayoshi (young)	35.478	133.910	1.34	3	**0.282914**	0.512639	0.705568	18.316	15.586	38.545	12.3		2.87	0.70	1.79	55.5	58	0.0155	1.04
KUR-01	Kurayoshi (young)	35.465	133.830	1.90	3	**0.283039**	0.512793	0.704720	18.218	15.550	38.347	8.52	**+5.68**	2.74	–0.27	1.66	57.4	54	0.0180	1.05
KUR-05	Kurayoshi (young)	35.461	133.861	1.13	3	**0.282946**	0.512680	0.705261	18.304	15.576	38.504	8.17	**+3.86**	2.80	0.93	2.18	50.6	55	0.0179	0.52
KUR-11	Kurayoshi (young)	35.470	133.802	1.24	3	**0.282988**	0.512822	0.704130	18.245	15.558	38.413	9.01	**+2.83**	3.34	0.25	1.49	60.0	54	0.0217	0.78
HMA type																				
JA-2	Setouchi	34.35	133.93	14.1		0.282876	0.512550	0.706370	18.394	15.598	38.668	28.7	**−1.00**	7.60	1.96	0.74	73.9	56		
TG1	Setouchi	34.46	135.56	13.9			0.512576	0.705127	18.446	15.606	38.672		**−0.12**	9.47	1.15	0.65	76.2	59		
SD264 (MDYB-2)	Setouchi	34.50	134.19	13.3		0.282981	0.512720	0.704861	18.366	15.594	38.552		**−0.26**	6.05	0.78	0.92	69.5	55		

Journal of Geophysical Research: Solid Earth
10.1029/2022JB025670

Table 1
Continued

Sample name	Region	Latitude (°N)	Longitude (°E)	Age (Ma)	Episode[a]	$(^{176}Hf/^{177}Hf)_t$	$(^{143}Nd/^{144}Nd)_t$	$(^{87}Sr/^{86}Sr)_t$	$(^{206}Pb/^{204}Pb)_t$	$(^{207}Pb/^{204}Pb)_t$	$(^{208}Pb/^{204}Pb)_t$	Li (μg·g^{-1})	δ^7Li	MgO (wt%)	LOI (wt%)	FeO[b]/MgO	Mg#[c]	CIA[d]	Cs/Rb	Li/Y
OIB type																				
ABU-28	Mishima	34.786	131.149	11.0	1	**0.282988**	0.512800	0.703843	17.780	15.498	37.971	8.26		7.41	1.27	1.09	65.8	57	0.0110	0.38
KAN-01	Kanmuri	34.437	132.077	11.0	1	**0.282815**	0.512653	0.704904	18.172	15.563	38.614	8.34		3.24	1.73	2.70	43.7	52	0.0119	0.41
KAN-03	Kanmuri	34.390	132.089	8.88	1	**0.282774**	0.512629	0.704727	18.062	15.552	38.686	8.16		5.02	0.44	2.16	49.2	54	0.0095	0.30
SER-05	Sera	34.640	132.903	9.38	1	**0.282835**	0.512679	0.704420	17.986	15.539	38.376	23.1		4.04	0.82	2.37	47.0	50	0.0489	0.91
SER-09	Sera	34.672	133.087	9.15	1	**0.282883**	0.512694	0.704838	18.119	15.547	38.415	9.61		7.45	0.60	1.41	59.9	55	0.0069	0.42
KIB-02	Kibi	34.911	133.345	8.57	1	**0.282884**	0.512734	0.704346	18.069	15.525	38.350	10.4		9.60	1.47	0.99	68.0	59	0.0376	0.48
KIB-05	Kibi	34.748	133.317	6.14	2	**0.282893**	0.512751	0.703970	17.945	15.484	38.243	7.13		9.70	0.93	1.08	65.9	53	0.0161	0.25
KIB-08	Kibi	34.740	133.378	8.0	2	**0.282919**	0.512752	0.704258	18.127	15.538	38.404	12.3		8.08	1.28	1.07	66.1	50	0.0251	0.58
SAM-01[e]	Hamada	35.037	132.560	6.13	2	**0.282896**	0.512704	0.705188	18.257	15.579	38.538	13.8		5.04	0.61	1.65	56.0	51	0.0499	0.49
HAM-03	Hamada	34.786	132.019	7.0	2	**0.282818**	0.512719	0.704281	17.669	15.501	38.324	5.69		14.43	1.23	0.75	73.8	52	0.0122	0.22
MY-01	Tsuyama	35.100	133.936	5.9	2	**0.282874**	0.512760	0.704831	18.105	15.525	38.316	8.97		8.72	1.33	1.11	65.3	56	0.0129	0.39
MY-02	Tsuyama	35.100	133.936	5.9	2	**0.282877**	0.512740	0.704562	18.099	15.519	38.299	13.0		9.09	1.89	1.05	66.6	58	0.0302	0.58
MY-03	Tsuyama	35.100	133.936	5.89	2	**0.282878**	0.512770	0.704394	18.096	15.517	38.311	11.5		8.86	0.42	1.13	64.9	53	0.0249	0.49
OY-01	Tsuyama	35.104	133.936	4.4	2	**0.282871**	0.512775	0.704513	18.189	15.532	38.372	14.8		8.02	3.54	1.23	63.0	60	0.0233	0.63
TSU-04	Tsuyama	35.054	134.109	6.64	2	**0.282892**						6.11		13.12	3.18	0.72	74.4	62	0.0264	0.30
ABU-16	Abu	34.440	131.584	0.31	3	**0.282972**	0.512822	0.704126	18.171	15.518	38.259	7.47		9.81	0.48	0.97	68.4	62	0.0184	0.45
KUR-09	Kurayoshi (young)	35.485	133.827	2.13	3	**0.282874**	0.512627	0.705809	18.335	15.592	38.586	13.0		5.84	−0.41	1.86	53.0	53	0.0131	0.63
KURA-01	Kurayoshi (young)	35.439	133.821	1.3	3	**0.282832**	0.512570	0.705930	18.336	15.588	38.574	10.9		4.34	0.43	2.40	46.7	58	0.0092	0.56
KURA-03	Kurayoshi (young)	35.442	133.838	1.34	3	**0.282863**	0.512594	0.705901	18.336	15.590	38.581	10.9		4.61	−0.64	2.23	48.4	57	0.0032	0.58
KURA-04	Kurayoshi (young)	35.442	133.838	1.3	3	**0.282832**	0.512546	0.706267	18.369	15.595	38.619	10.2		4.72	−1.31	2.27	48.0	56	0.0076	0.44
DAIK-02	Daikonjima	35.486	133.183	0.1	3	**0.282850**	0.512658	0.704557	17.961	15.536	38.385	6.12		7.41	0.85	1.41	59.8	64	0.0075	0.33
DAIK-03	Daikonjima	34.437	132.077	0.10	3	**0.282795**	0.512555	0.704708	17.908	15.548	38.399	8.22		6.66	1.32	1.49	58.5	64	0.0196	0.52
OGI-12	N. Hyogo	35.511	133.189	1.09	3	**0.282778**	0.512500	0.707136	18.352	15.597	38.637	10.0		6.09	0.22	1.67	55.7	57	0.0127	0.53
HYO-09	N. Hyogo	35.472	134.786	0.14	3	**0.282882**	0.512692	0.704781	18.106	15.554	38.383	7.50		7.35	0.19	1.47	58.8	59	0.0163	0.28
HYO-11	N. Hyogo	35.488	134.701	0.09	3	**0.282875**	0.512664	0.705001	18.144	15.552	38.400	8.84		6.67	−0.48	1.61	56.6	55	0.0154	0.33
HYO-14	N. Hyogo	35.582	134.777	1.52	3	**0.282842**	0.512576	0.706565	18.345	15.594	38.624	9.59		6.50	−0.03	1.45	59.2	55	0.0085	0.47
Yakuno	N. Hyogo	35.329	134.936	0.4	3	**0.282785**	0.512457	0.707316	18.314	15.583	38.578	11.8		4.90	−0.92	2.03	50.9	58	0.0156	0.57

Note: Analyses shown by boldface font were obtained in this study, and those shown by normal font were obtained by Feineman et al. (2013), Imai et al. (1995); Ishikawa and Nakamura (1994), Ishizaka and Carlson (1983), Nguyen et al. (2020), Pineda-Velasco et al. (2018), Tatsumi and Ishizaka (1982a, 1982b), and Shimoda et al. (1998).

[a]Episode 1, 12–8 Ma; Episode 2, 8–4 Ma; Episode 3, 4 Ma to present (Nguyen et al., 2020). [b]Total Fe as FeO. [c]Mg# value is calculated as 100 Mg/(Mg + Fe^{2+}) where Fe^{2+}/Fe_{total} is assumed to be 0.80 for ADK (Pineda-Velasco et al., 2018) and 0.85 for HMA, IAB and OIB (Nguyen et al., 2020; this study). [d]Chemical index of alteration (CIA) after McLennan (1993) and Nesbitt and Young (1982), defined as $[Al_2O_3/(Al_2O_3 + CaO^* + Na_2O + K_2O)] \times 100$ where oxide abundances are given in molecular proportions and CaO* denotes CaO abundances in silicate fraction in a rock. [e]The sample name of "SAM-01" is assigned to different rock specimens; one for ADK-type dacite from Sambe volcano and another is OIB-type basalt from the vicinity of Sambe volcano (Nguyen et al., 2020; Pineda-Velasco et al., 2018).

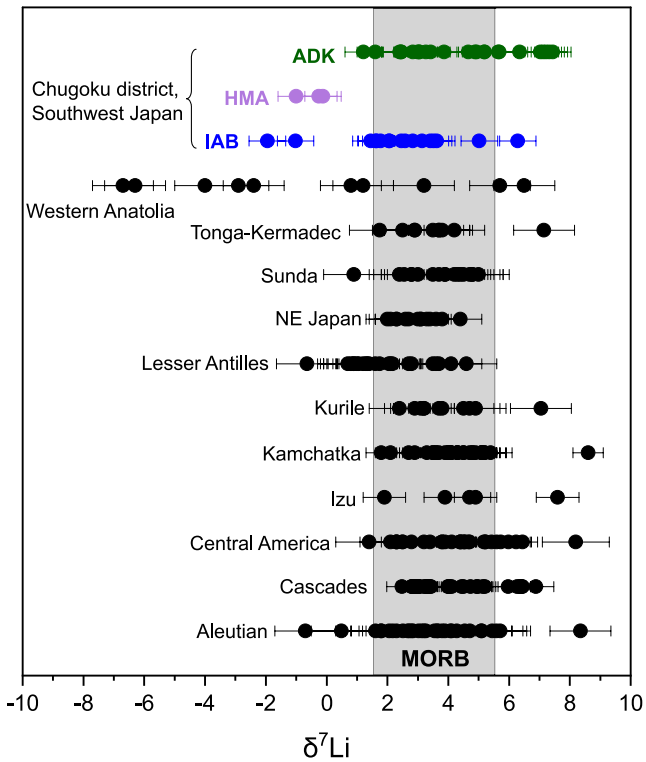

Figure 2. δ^7Li values in volcanic rocks from the Chugoku district in SW Japan (ADK: green dots; HMA: purple dots; IAB: blue dots) compared to published values for mafic-intermediate volcanic rocks ($SiO_2 \leq 63$ wt%, except for rocks classified as "adakite") in other arcs. Note that the data for altered rocks or atypical arc rocks are screened out; those include rocks with high LOI (loss on ignition) or high CIA (chemical index of alteration), highly alkaline rocks (e.g., shoshonite), and intraplate-type mafic rocks (similar to our OIB). The range of δ^7Li values of unaltered MORB is shown as a gray band ($+1.6‰ \leq \delta^7Li \leq +5.6‰$; H. R. Marschall et al., 2017; Tomascak et al., 2008). Data sources of the δ^7Li values of other arc volcanic rocks are as follows; Aleutians (Hanna et al., 2020; Tomascak et al., 2002), Cascades (Leeman et al., 2004; Magna, Wiechert, Grove, et al., 2006), Central America (Chan et al., 2002; Tomascak et al., 2000; Walker et al., 2009), Izu (Moriguti & Nakamura, 1998), Kamchatka (Halama et al., 2009; Liu et al., 2020), Kurile (Tomascak et al., 2002), Lesser Antilles (Tang et al., 2014), NE Japan (Moriguti et al., 2004), Sunda (Tomascak et al., 2002), Tonga-Kermadec (Brens et al., 2019), Western Anatolia (Agostini et al., 2008). Analytical uncertainties of δ^7Li values (as 2σ external reproducibility or $2\sigma_m$ within-run precision) are shown as error bars (0.6‰ for our study, and 0.07–1.2‰ for the literature data).

volcanic rocks from global arcs (Figure 2). An exception is the Western Anatolia-Aegean arc that contains Cenozoic mafic-intermediate volcanic rocks with extremely low and high δ^7Li values (−7.0‰ to +8.2‰; Agostini et al., 2008). In the arc, the difference in δ^7Li value among samples is related to rock suites. The low-δ^7Li volcanic rocks (−7.0‰ to +3.2‰) are from the ultrapotassic suite, while the high-δ^7Li volcanic rocks (+5.7 to +8.2‰) are from the sub-alkaline andesitic suite. Owing to their significant δ^7Li variation, SW Japan lavas may provide a vital opportunity to examine the role of slab contribution and slab-mantle interaction in Li isotopic systematics.

We first discuss whether the processes responsible for the large variation in δ^7Li of the Chugoku volcanic rocks occurred at a shallow level (e.g., intracrustal) or deep level (e.g., mantle) (Section 5.1). Then, we discuss the δ^7Li variation via (a) sediment and altered oceanic crust (AOC) contributions (Section 5.2), and (b) Li-isotope fractionation during subduction (Section 5.3). Then, we address the interaction of slab-derived components and the mantle (Section 5.4). Finally, we provide the implication of δ^7Li variation in global arc magmas (Section 5.5).

5.1. Processes Responsible for ^{7}Li/^{6}Li Variation

5.1.1. Post-Emplacement Processes

Fractionation of ^{6}Li and ^{7}Li could occur by degassing of magmas during their emplacements (Neukampf et al., 2022; Schiavi et al., 2010). During degassing of felsic melts, Li is partitioned into a vapor (fluid) phase (Webster et al., 1989). Fractionation of ^{6}Li and ^{7}Li via degassing also results in the depletion of ^{7}Li in a residual melt, and thus the [Li] and δ^7Li values of co-magmatic samples show a positive correlation (e.g., Neukampf et al., 2022). Such a positive correlation is not observed in IAB or ADK rocks from each volcanic field (Figure S1 in Supporting Information S1). Thus, the δ^7Li variations in these rocks are dominantly controlled by processes other than degassing.

Post-emplacement weathering is also considered to alter the δ^7Li values of volcanic rocks by the uptake of Li into clay minerals formed by alteration of primary silicates (e.g., Vigier et al., 2008). Between clay minerals and a fluid, isotope fractionation occurs, resulting in enrichment of ^{6}Li in altered silicate rocks containing clay minerals (Vigier et al., 2008). Clay minerals form from primary volcanic constituents, and their formations accompany a net loss of the mobile elements, including Mg, Ca, Na and K. By contrast, Al and Fe are preferentially retained in weathered rocks (Babechuk et al., 2014). Accordingly, relative proportions of major element oxides show the variations among rocks with different extents of weathering and alteration. The chemical index of alteration (CIA), given as molar fractions of major oxides $Al_2O_3/(Al_2O_3 + CaO^* + Na_2O + K_2O) \times 100$ (where CaO* refers to Ca in silicates) represents a good measure of the extent of weathering/alteration (McLennan, 1993; Nesbitt & Young, 1982). The δ^7Li and CIA values of ADK and IAB samples in each volcanic field do not show a clear correlation (Figure 4a and Figure S2 in Supporting Information S1). Secondary alteration could also result in elemental fractionation, resulting in variations in Cs/Rb and Li/Y, owing to different susceptibility or resistivity against secondary alteration (Palmer & Edmond, 1989; Seyfried et al., 1998). These element ratios are not correlated with δ^7Li (Figure S3 in Supporting Information S1), providing further support for an insignificant effect of secondary alteration on δ^7Li variations in IAB and ADK. In summary, the observed variation in δ^7Li of the volcanic rocks in the Chugoku district is largely attributed to the processes that occurred prior to the eruption of their parent magmas (Text S2 in Supporting Information S1).

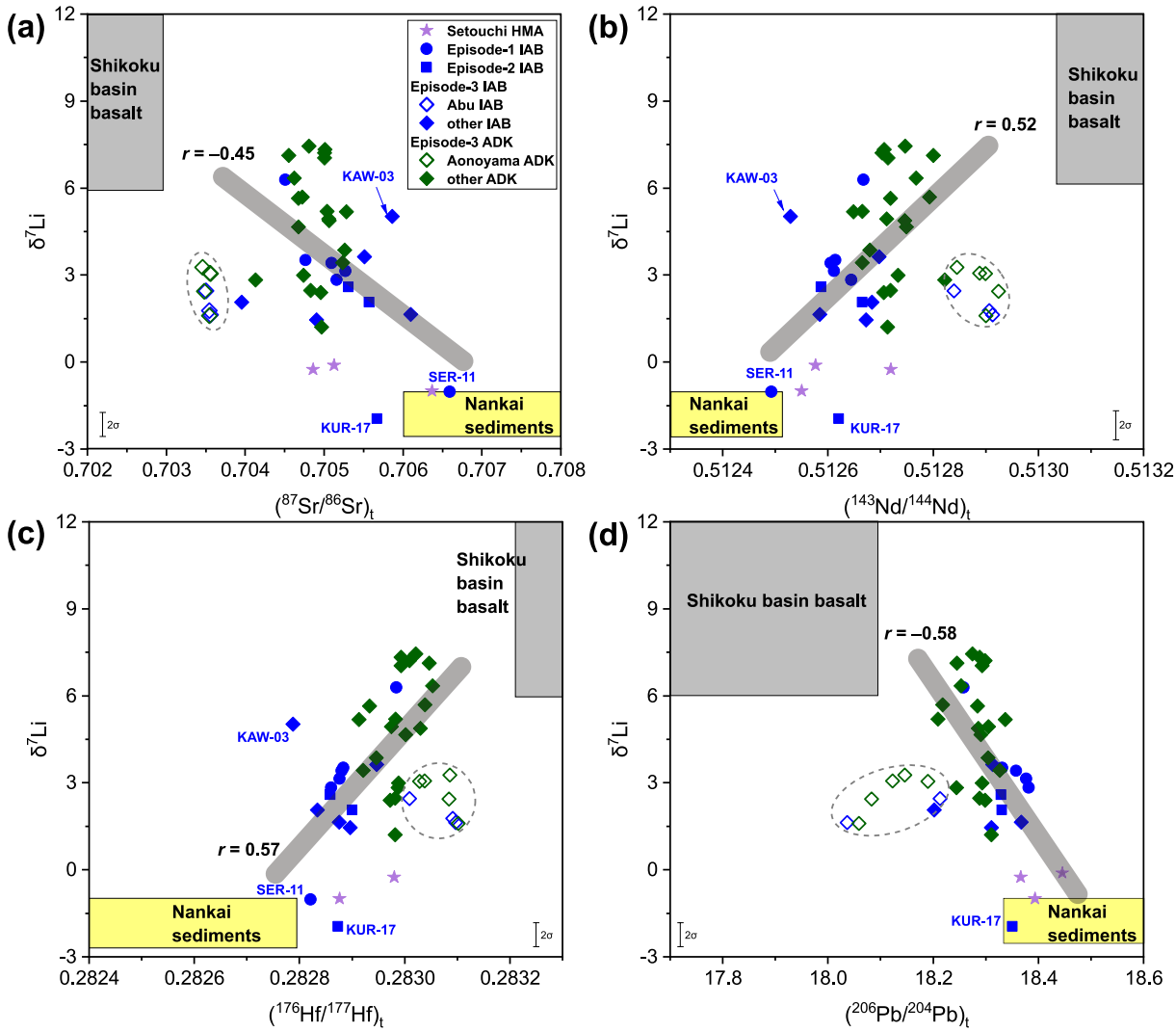

Figure 3. Plot of δ^7Li in volcanic rocks from the Chugoku district in SW Japan versus (a) $(^{87}Sr/^{86}Sr)_t$, (b) $(^{143}Nd/^{144}Nd)_t$, (c) $(^{176}Hf/^{177}Hf)_t$, and (d) $(^{206}Pb/^{204}Pb)_t$. Correlation coefficients (r) for δ^7Li values and Sr-Nd-Hf-Pb isotopic compositions are shown in each plot (Note that r is calculated for IAB and ADK shown by filled symbols. Data shown by open symbols [Aonoyama and Abu rocks], enclosed by dashed line, are excluded for this evaluation). Sr-Nd-Pb-Hf isotopic data of the Chugoku volcanic rocks are from Nguyen et al. (2020) and Pineda-Velasco et al. (2018). δ^7Li values of subducted sediments are taken from the δ^7Li values measured by Moriguti and Nakamura (1998) for metasedimentary rocks (shales) in the accretionary complex (Shimanto Belt). Sr-Nd-Pb-Hf isotopic compositions of sediments are from published data for the Shimanto shales/sand stones or terrigenous sediments in Nankai Trough/Shikoku Basin (Ishikawa & Nakamura, 1994; Plank & Langmuir, 1998; Shimoda et al., 1998; Shu et al., 2017; Terakado et al., 1988). Sr-Nd-Pb-Hf isotope compositions of Shikoku basin basalts are from Hickey-Vargas (1991, 1998), Ishizuka et al. (2009), Shu et al. (2017), and Straub et al. (2010). The range of δ^7Li values in Shikoku Basin basalts is assumed to be the same as the variation in global seafloor basalts (i.e., altered oceanic crusts) presented in Penniston-Dorland et al. (2017). δ^7Li value of mantle wedge is assumed to be $+3.5 \pm 0.5‰$, which is the mean δ^7Li value of pristine peridotites (Jeffcoate et al., 2007; Lai et al., 2015; Magna, Wiechert, & Halliday, 2006; Pogge von Strandmann et al., 2011; Seitz et al., 2004). Uncertainty of δ^7Li values for the Chugoku district samples is $\pm 0.6‰$ (2σ external reproducibility).

5.1.2. Pre-Emplacement Processes

It is generally considered that fractionation of ^{7}Li/^{6}Li occurs to a limited extent in magmatic systems, owing to a high diffusion rate at high temperatures (~1,000°C) (Schuessler et al., 2009; Tomascak et al., 1999). During differentiation of a magma, Li exchanges between crystallized phases (e.g., olivine and clinopyroxene) and a residual magma. Li-isotope fractionation associated with kinetic process is complex. Numerical experiments or in-situ analyses of Li-isotope compositions demonstrated that the δ^7Li values of these phases could decrease by 10‰ or more relative to a coexisting melt (Parkinson et al., 2007; Weyer & Seitz, 2012). Residual magma

may become enriched in ^{7}Li by mechanical separation of these phases if a magma body is relatively small. However, such a process is unlikely to significantly affect the δ^{7}Li values of volcanic rocks because the faster and continuous diffusion of Li rapidly attenuates Li-isotope profile within crystallized phases prior to eruptions (Dohmen et al., 2010). Thus, it is unlikely that magmatic differentiation is responsible for production of the entire δ^{7}Li variation (>9‰) in the Chugoku volcanic rocks. This inference is supported by covariation of δ^{7}Li values with the Sr, Nd, Hf and Pb isotopic compositions of these rocks. Nevertheless, we examine the feasibility of Li isotope fractionation via magmatic processes.

In Figure 4b, the δ^{7}Li values of IAB and ADK are plotted against their MgO contents, as indices of differentiation. Although our samples were collected from volcanoes in different fields in the Chugoku district, an overall correlation between the δ^{7}Li value and MgO content is anticipated if the variation in δ^{7}Li is dominated by fractional crystallization. However, these rocks do not show a significant correlation ($r = -0.057$ for ADK and -0.016 for IAB) between δ^{7}Li and MgO, even among samples from the same volcanic fields (Figure 4b and Figure S4 in Supporting Information S1). We thus consider that the variation in δ^{7}Li of the Chugoku volcanic rocks was produced by processes other than fractional crystallization, consistent with the conclusion of previous studies (Schuessler et al., 2009; Tomascak et al., 1999).

The δ^{7}Li value of a magma could also be altered via ingestion of crustal materials with distinct δ^{7}Li values. Crustal materials in the Chugoku district mainly consist of felsic plutonic rocks in its upper part and mafic plutonic rocks in its lower part (Yamane et al., 2012). Felsic plutonic rocks are considered to be a major assimilant since they have solidus temperatures lower than those of mafic magmas. A reference silicate rock, JG-3, provided by the Geological Survey of Japan, is a Paleogene (58–56 Ma) granodiorite from the Chugoku district (Ishihara & Tani, 2013; Noguchi et al., 2021). This rock could represent a felsic member of the upper crustal rock in the Chugoku district. The [Li] of 20.9 and 24.5 $\mu g \cdot g^{-1}$ and the δ^{7}Li value of +2.40 and +2.56‰ are reported for JG-3 (Magna et al., 2010; Figure 4b). The δ^{7}Li values of the JG-3 aliquots are well within the range of δ^{7}Li values of the volcanic rocks from the Chugoku district as well as that of unaltered MORB. Accordingly, assimilation of upper crustal rock in mafic magmas could not produce intermediate to felsic magmas with the δ^{7}Li values significantly different from MORB. The ADK-type andesites and dacites dominate intermediate and felsic volcanic rocks erupted in Episode 3 (Kimura et al., 2005), and their δ^{7}Li values (−2.0 to +6.3‰) significantly overlap with the δ^{7}Li values of IAB in the same episode (+1.5 to +5.0‰). Thus, one may anticipate that ADK could have been derived by fractional crystallization of mafic parental magmas with or without the assimilation of upper crustal rocks. Previous studies, however, suggest that ADK magmas were derived by melting of the subducted oceanic lithosphere (Feineman et al., 2013; Kimura et al., 2014; Pineda-Velasco et al., 2018). We thus consider that crustal assimilation did not play a major role in the production of δ^{7}Li variation among different types of volcanic rocks in the Chugoku district.

5.1.3. Subduction Inputs to the Magma Sources

Neither post-emplacement alteration nor pre-emplacement magmatic processes account for the observed δ^{7}Li variations in the Chugoku volcanic rocks. We thus infer that δ^{7}Li variations reflect the characteristics of their magma sources or the processes of melt transport in the mantle. Nguyen et al. (2020) argued that polybaric melting of upwelling mantle resulted in the predominance of refractory peridotite in the wedge mantle. The δ^{7}Li value of the mantle would have varied little since peridotite represents a major source of Li in the mantle. We thus assume the δ^{7}Li value of the wedge mantle to be the same as the mean δ^{7}Li value (+3.5 ± 1.0‰) of pristine peridotites (Jeffcoate et al., 2007; Lai et al., 2015; Magna, Wiechert, & Halliday, 2006; Pogge von Strandmann et al., 2011; Seitz et al., 2004). It is noted that the δ^{7}Li value postulated for the wedge mantle is identical to the mean δ^{7}Li value of unaltered MORB (+3.6 ± 2.0‰) within analytical uncertainty. The δ^{7}Li value of the Chugoku volcanic rocks extends beyond the postulated δ^{7}Li value of the mantle, implying the contribution of the other magma sources.

The other sources are likely derived from crustal or lithospheric materials introduced into melting regions via slab subduction (Feineman et al., 2013; Kimura et al., 2014; Nguyen et al., 2020; Pineda-Velasco et al., 2018). We considered that these sources include AOC, sediments, and/or serpentinite (e.g., Liu et al., 2020; Moriguti & Nakamura, 1998; Tang et al., 2014). The HMA and ADK provide key constraints to identify the contributions

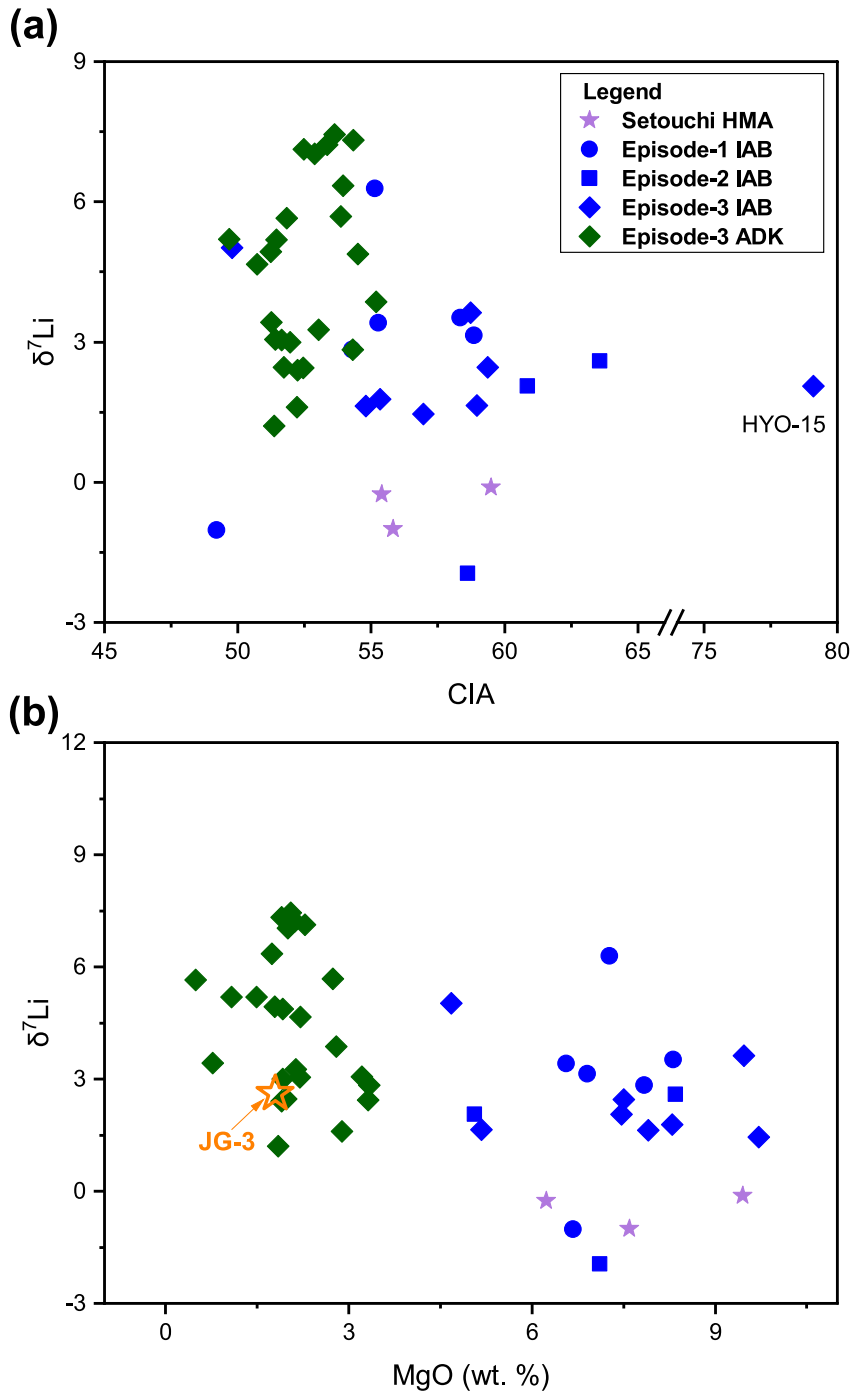

Figure 4. Plots of δ^7Li in ADK and IAB of the Chugoku district in SW Japan against (a) CIA (chemical index of alteration; $Al_2O_3/(Al_2O_3 + CaO^* + Na_2O + K_2O) \times 100$, where CaO* refers to Ca in silicates [McLennan, 1993; Nesbitt & Young, 1982]) and (b) MgO. The composition of JG-3, an upper-crustal granitic rock in the Chugoku district, is from Imai et al. (1995) and Magna et al. (2010). Uncertainty of δ^7Li values of the Chugoku district samples is ±0.6‰ (2σ external reproducibility).

of these components. HMA is considered to have been mainly derived from subducted sediments (Hanyu et al., 2002; Kawamoto et al., 2012; Shimoda et al., 1998; Tatsumi & Hanyu, 2003), whereas ADK is suggested to have been largely derived from AOC (Feineman et al., 2013; Kimura et al., 2014; Pineda-Velasco et al., 2018; Text S4 in Supporting Information S1). These volcanic rocks show significant variations in Sr-Nd-Hf-Pb isotope compositions, which are interpreted to have resulted from the changes in relative contributions of AOC and

sediments to parental magmas (Feineman et al., 2013; Hanyu et al., 2002; Kimura et al., 2014; Pineda-Velasco et al., 2018; Shimoda et al., 1998; Tatsumi & Hanyu, 2003). Thus, the comparison of Li-isotope data with Sr-Nd-Hf-Pb isotope data for these samples may provide insights into the δ^7Li signatures of AOC and sediments subducted beneath the Chugoku district. For this purpose, δ^7Li values of the IAB, ADK and HMA are plotted against $^{87}Sr/^{86}Sr$, $^{143}Nd/^{144}Nd$, $^{176}Hf/^{177}Hf$, and $^{206}Pb/^{204}Pb$ ratios in Figure 3. In these plots, broad correlations are observed; positive correlations are found between δ^7Li values and $^{143}Nd/^{144}Nd$ and $^{176}Hf/^{177}Hf$ ratios, while negative correlations are found between δ^7Li values and $^{87}Sr/^{86}Sr$ and $^{206}Pb/^{204}Pb$ ratios, respectively. If data for ADK from Aonoyama (6 out of 6 samples) and IAB from Abu (6 out of 6 samples) are excluded, the correlations are considered to be significant; absolute values of correlation coefficients for these pairs are 0.45–0.58 (Figure 3) and the statistic t for these coefficients are 2.99–4.13 which are greater than the critical t value at 5% significance level ($t_{critical}$ = 2.030–2.035 for degree of freedom of N_{data} − 2 [35–37]). These linear correlations point toward the compositions of AOC (Shikoku Basin basalts; Hickey-Vargas, 1991, 1998; Ishizuka et al., 2009; Shu et al., 2017; Straub et al., 2010) and sediments (Nankai sediments; Ishikawa & Nakamura, 1994; Moriguti & Nakamura, 1998; Plank & Langmuir, 1998; Shimoda et al., 1998; Shu et al., 2017; Terakado et al., 1988; You et al., 1995). The ADK and HMA samples plot close to these compositions. We thus consider that these two magma types preserve a slab-derived Li-isotope signature, although their parental magmas must have interacted with wedge mantle to different extents, inferred from large differences in MgO content or $Mg^{\#}$ between these two magma types; MgO = 0.36–3.3 wt% and $Mg^{\#}$ = 25–61 for ADK, and MgO = 6.1–9.5 wt% and $Mg^{\#}$ = 70–76 for HMA (Table 1; Pineda-Velasco et al., 2018; Tatsumi & Ishizaka, 1982a).

It should be also noted that the samples excluded for the above evaluation show distinct geochemical features. Aonoyama ADK and Abu IAB show larger variations in $^{143}Nd/^{144}Nd$ and smaller variations in $^{87}Sr/^{86}Sr$ than other ADK and IAB (Kimura et al., 2014). Pineda-Velasco et al. (2018) interpreted that the difference in the $^{143}Nd/^{144}Nd$-$^{87}Sr/^{86}Sr$ correlation between Aonoyama and other ADK samples is due to smaller extent of melting of AOC beneath Aonoyama (and adjacent Abu) region(s). The data for Aonoyama ADK and Abu IAB plot off the arrays formed by the other ADK and IAB to lower $^{87}Sr/^{86}Sr$ and $^{206}Pb/^{204}Pb$ and to higher $^{143}Nd/^{144}Nd$ and $^{176}Hf/^{177}Hf$ (Figure 3). Possible causes of their derivations from the isotope-correlation arrays are discussed in Section 5.4.

5.2. Processes Responsible for Heterogeneity of Li Isotope Compositions of the Chugoku Magmas

Volcanic rocks (mafic to intermediate) in different arcs show different extents of the variations in δ^7Li values (Figure 2). The rocks in some arcs show the δ^7Li variation mostly falling within the δ^7Li range of unaltered MORB. The arcs dominated by volcanic rocks with δ^7Li values of +1.6 to +5.6‰ are Aleutian (Hanna et al., 2020; Tomascak et al., 2002), Kamchatka (Liu et al., 2020), NE Japan (Moriguti et al., 2004), Sunda (Tomascak et al., 2002), and Tonga-Kermadec (Brens et al., 2019). In these arcs, the δ^7Li data for 85% or more samples fall within the range of δ^7Li values of unaltered MORB. Volcanic rocks in some back-arc basins also yield mafic volcanic rocks with δ^7Li values mostly within the range of MORB (e.g., South Shetland [Ross Island; Košler et al., 2009], Ryukyu [Okinawa Trough; Zeng et al., 2021], and Tonga [Lau Basin; Brens et al., 2019]).

By contrast, some arcs contain volcanic rocks with δ^7Li values higher than that of unaltered MORB (>+5.6‰) in a significant proportion. These arcs include Cascades (7 out of 30; Leeman et al., 2004; Magna, Wiechert, Grove, et al., 2006) and Central America (6 out of 33; Chan et al., 2002; Tomascak et al., 2000; Walker et al., 2009). Minor occurrences of high-δ^7Li rocks are also found in some arcs (e.g., Izu with 1 out of 5 samples; Moriguti & Nakamura, 1998). Also noted are the other two arcs which contain volcanic rocks with δ^7Li values lower than unaltered MORB (<+1.6‰) in a significant proportion. These arcs are Lesser Antilles (11 out of 23 samples; Tang et al., 2014) and Western Anatolia (7 out of 10 samples Agostini et al., 2008). Such low-δ^7Li rocks are also found in the Chugoku district (HMA and a few IAB rocks). The Chugoku district is also characterized by the occurrence of volcanic rocks with δ^7Li values higher than unaltered MORB in a significant proportion (9 of 42 samples).

In general, volcanic rocks show across-arc variations in abundance ratios of key trace elements (e.g., Li/Y, B/Be, B/Nb, Ce/Pb, Ba/La) and $^{87}Sr/^{86}Sr$, $^{143}Nd/^{144}Nd$, $^{176}Hf/^{177}Hf$ and $^{206,\ 207,\ 208}Pb/^{204}Pb$. The variations in these trace-element and isotopic ratios extend beyond the ranges found in MORB. Such large variations are interpreted as a result of the involvement of subducted materials (AOC and sediments) in magma sources (e.g.,

Ishikawa & Nakamura, 1994; Nakamura et al., 1985; Perfit et al., 1980; Sakuyama & Nesbitt, 1986; Shibata & Nakamura, 1997; Yogodzinski et al., 2015; Yokoyama et al., 2003). Hence, these trace-elements and isotopic ratios have been used as geochemical proxies of the subduction inputs. It is noted that the δ^7Li values of volcanic rocks in most arcs do not show clear correlations with the above trace-element and isotopic ratios (e.g., Hanna et al., 2020; Leeman et al., 2004; Moriguti et al., 2004; Tang et al., 2014).

Apparent similarity of δ^7Li values between arc volcanic rocks and unaltered MORB has been attributed to (a) mixing of slab-derived components and mantle, both of which have similar δ^7Li values (i.e., sediments have δ^7Li values falling within the range of unaltered MORB; e.g., Brens et al., 2019; Tang et al., 2014), (b) no or insignificant Li inputs from a subducting slab after intensive dehydration at shallower depths (it lost most of its Li; e.g., Leeman et al., 2004; Magna, Wiechert, Grove, et al., 2006), (c) buffering of slab-derived Li via isotopic exchange with surrounding mantle (with δ^7Li value falling within the range of unaltered MORB; e.g., Caciagli et al., 2011; Halama et al., 2009). These three scenarios could also explain the lack of clear correlations between δ^7Li values and trace-elements and Sr-Nd-Hf-Pb isotopic ratios.

Scenario 1 is suggested in the studies of the volcanic rocks in the Tonga-Kermadec arc (Brens et al., 2019) and Aleutian arc (Hanna et al., 2020). Considering their high [Li] ($\sim$100 $\mu g \cdot g^{-1}$; Brens et al., 2019; Plank, 2014; Tang et al., 2014), subducted sediments could represent one of the major Li inputs in arc-magma sources. In the studies of volcanic rocks from these arcs, the δ^7Li values of subducting sediments are directly measured (Brens et al., 2019; Chan et al., 2006). The δ^7Li values of these sediments show a variation of +1.2 to +8.0‰; that is, most of them have δ^7Li values indistinguishable from unaltered MORB (+1.6 to +5.6‰; H. R. Marschall et al., 2017; Tomascak et al., 2008). The δ^7Li value of the global subducting sediment, given as a weighted mean of the analyses for 27 trench sediments, is +2.4 ± 0.2‰ (Plank, 2014), being well within the range of δ^7Li of unaltered MORB (+3.6 ± 2.0; Tomascak et al., 2008). Therefore, if Li inventory in arc magmas is dominated by subducting sediments, volcanic rocks in those arcs should have δ^7Li values indistinguishable from MORB. In this case, arc magmas are expected to show marked enrichments of trace elements such as Ba, Pb and Th (Plank, 2014).

Scenario 2 is suggested in the studies of volcanic rocks in NE Japan (Moriguti et al., 2004) and Cascadia arcs (Leeman et al., 2004; Magna, Wiechert, Grove, et al., 2006). These island arcs have subducting slabs with shallower dip angles or younger ages, thus intensive dehydration would have occurred at shallower depths due to a high *T*/*P* gradient via subduction. During dehydration, ^{7}Li should have been lost preferentially from subducted AOC or sediments. For AOC, progressive dehydration may have lowered its δ^7Li, and eventually it could have δ^7Li values indistinguishable from the wedge mantle. Further dehydration of deeply subducted AOC could have δ^7Li values lower than that of unaltered MORB (<+1.6‰). The occurrence of low-δ^7Li metamorphic rocks in exhumed subduction complexes (Simons et al., 2010; Zack et al., 2003) or low-δ^7Li magmas (melt inclusions) in plume-related volcanic fields (Kobayashi et al., 2004) and ultra rear-arc regions (Schiavi et al., 2012) may support this inference.

Scenario 3 is suggested in the studies of volcanic rocks in Kurile, Sunda, Aleutians (Tomascak et al., 2002) and Kamchatka (Liu et al., 2020). In these arcs, significant contributions from subducted slabs are detected by various geochemical proxies (e.g., Li/Y, B/Be, B/Nb, Ba/La, Pb/Ce, Sb/Ce). In addition, these proxies show significant variations within each arc and often exhibit clear across-arc trends. Apparent decoupling of the δ^7Li values and other trace-element ratios can be explained by buffering of isotopic differences between slab-derived Li and mantle Li via diffusive equilibration (Caciagli et al., 2011; Halama et al., 2009). This in turn suggests that travel time of slab-derived fluids to magma source regions is long enough to attain diffusive isotope equilibrium in most arcs.

The Chugoku volcanic rocks show variation in their δ^7Li value that extends beyond the range of MORB. Thus, the processes mentioned in Scenario 1 did not occur or occurred but did not affect the Li isotopic compositions of the magmas. The process mentioned in Scenario 2 (i.e., intensive dehydration) likely occurred, as the current PHS slab is subducting at a shallow angle. Isotope equilibration via fluid-mantle interaction, as proposed in Scenario 3, may also have occurred to some extent. However, neither Scenarios 2 nor 3 did completely attenuate slab-derived Li-isotope signatures found in the Chugoku volcanic rocks. The origin of the δ^7Li variation in the volcanic rocks is attributed to the involvement of multiple Li inventories. We discuss possible Li inventories in Sections 5.2.1–5.2.3 to examine Scenario 1. Then, Li-isotope fractionation during subduction is discussed in

Section 5.3 to examine Scenario 2. Lastly, the effect of the process proposed in Scenario 3, that is, mantle buffering, is discussed in Section 5.4.

5.2.1. Sediments

Sedimentary rocks in the Nankai Trough or fore-arc terrane have δ^7Li values of −4.5 to +4.6‰, and the majority have δ^7Li < +2‰ (Moriguti & Nakamura, 1998; You et al., 1995; Text S4.1 in Supporting Information S1). It has been argued that the Setouchi HMA was derived from a source largely affected by sediments (Hanyu et al., 2002; Kawamoto et al., 2012; Shimoda et al., 1998). Their δ^7Li values (−1.0 to −0.2‰) are significantly lower than those of unaltered MORB, while these values are well within the range of sediments. Thus, the sediment origin for this magma is supported by Li-isotopic compositions (Oi et al., 1997; this study). The eruption of the Sera lamprophyre occurred shortly (~2 Myrs) after the eruption of HMA. The δ^7Li value of the rock (−1.0‰) is also lower than MORB (Figure 3). This peculiar high-K rock has geochemical features consistent with its derivation from a sediment-enriched source (e.g., strong enrichments in Ba, Th, Pb, REE and Li; Nguyen et al., 2020). We thus consider that sediments subducted beneath the Chugoku district have δ^7Li values significantly lower than those of unaltered MORB.

Previous studies proposed that ADK in the Chugoku district was produced by the melting of subducted oceanic crust with significant sediment contribution (Feineman et al., 2013; Kimura et al., 2014; Pineda-Velasco et al., 2018). However, ADK have δ^7Li values different from sediments. Rather, these are similar to the δ^7Li values of unaltered MORB or AOC (Figure 3). The apparent discrepancy of the sediment contribution to ADK will be examined in Section 5.4 using Li isotope data from this study and Sr-Nd-Pb isotope composition by Feineman et al. (2013) and Pienda-Velasco et al. (2018).

5.2.2. AOC

Previous studies have documented that IAB and ADK show broad linear correlations among their Sr, Nd, Hf and Pb isotope compositions and these linear or curvilinear arrays in a plot point toward the compositions of subducted basalts and sediments (Feineman et al., 2013; Kimura et al., 2014; Nguyen et al., 2020; Pineda-Velasco et al., 2018). New δ^7Li data for IAB and ADK samples from this study are combined with Sr, Nd, Hf and Pb isotope data published in these previous studies (Figure 3). Broad linear correlations are also observed between δ^7Li values and ^{87}Sr/^{86}Sr, ^{143}Nd/^{144}Nd, ^{176}Hf/^{177}Hf or ^{206}Pb/^{204}Pb ratios. The lower δ^7Li ends of these linear arrays point toward the measured composition of Nankai sediments. Therefore, the higher δ^7Li ends of these arrays are interpreted to represent the compositions of AOC. This inference is consistent with the estimated Sr, Nd, Hf and Pb isotopic compositions (lower ^{87}Sr/^{86}Sr and ^{206}Pb/^{204}Pb ratios and higher ^{143}Nd/^{144}Nd and ^{176}Hf/^{177}Hf ratios) similar to the observed compositions of the Shikoku-Basin basalts. We estimated the [Li] and δ^7Li values to be 16 μg·g^{-1} and +11.3‰ for AOC before subduction (Text S4.1 in Supporting Information S1).

5.2.3. Serpentinized Mantle

Some ADK have δ^7Li values significantly higher than unaltered MORB. This feature can also be explained if a high-δ^7Li source(s) other than AOC was involved. Pineda-Velasco et al. (2018) argued that the fluids that facilitated slab melting may have been supplied from sub-surface layers (mantle section) of the subducting lithosphere. Serpentinite, a major lithology of the slab mantle section, could retain fluids to a deeper level (~100 km or deeper) if it was not intensively heated (<700°C; Ulmer & Trommsdorff, 1995). Thus, it can be a main fluid supplier other than AOC. Pineda-Velasco et al. (2018) noted that ADK volcanoes are located above aseismic slab discontinuities (Figure 1), interpreted as slab tears at, which the slab mantle section was exposed to ambient asthenospheric mantle. Exposure to asthenospheric mantle may have caused intensive dehydration of this layer and induced melting of the overlying AOC layer. Serpentinized abyssal peridotites have a greater variation in δ^7Li values (−28 to +14‰) than their unaltered protoliths, and higher δ^7Li values (δ^7Li > +5.6‰) are found in rocks with higher [Li] (0.5–9 μg·g^{-1}; Decitre et al., 2002; Vils et al., 2009). If the subducted PHS plate contained a high-δ^7Li serpentinized section, then the breakdown of serpentines in the section could have resulted in the release of fluids that could facilitate the melting of AOC and elevate the δ^7Li values of AOC melts. It is however noted that [Li] in serpentinized abyssal peridotites are generally low (3.3 ± 3.0 μg·g^{-1} [n = 6], calculated for rocks with δ^7Li > +5.6‰ in Decitre et al. (2002) and Vils et al. (2009)), compared with [Li] of AOC (6–37 μg·g^{-1}; Chan et al. (2002); Bouman et al. (2004)). In addition, released Li is mostly redistributed in olivines in solid residues after the dehydration of serpentinite (Scambelluri et al., 2004). Accordingly, [Li] in fluids is buffered at a lower level. We thus conclude that serpentinite dehydration would have little

affected the δ^7Li value of ADK. Instead, high δ^7Li values in ADK should be explained as a result of limited or insignificant fractionation of ^{7}Li/^{6}Li in AOC during the metamorphic dehydration of the subducted slab.

5.3. Li-Isotope Fractionation During Subduction

SW Japan arc is a hot subduction zone where a young oceanic lithosphere is subducting (Syracuse et al., 2010; van Keken et al., 2011). Therefore, intensive dehydration of AOC and sediment (SED) should have occurred during subduction (Peacock & Wang, 1999; Tatsumi et al., 2020). Intensive dehydration should have induced Li isotope fractionation (H. R. Marschall et al., 2007; Simons et al., 2010; Zack et al., 2003). Zack et al. (2003) examined the evolution of δ^7Li in subducting AOC using a simple Rayleigh distillation model with a constant isotope fractionation factor and partition coefficient between rocks and fluids (Text S4.2 and Figure S6 in Supporting Information S1). However, such a simple model is probably not viable, as AOC and SED would have dehydrated continuously during subduction. Given that fractionation factor and partition coefficient would have varied, owing to changes in *P-T* condition via subduction (Berger et al., 1988; H. R. Marschall et al., 2007; Wunder et al., 2006), it is more appropriate to apply the incremental dehydration model (H. R. Marschall et al., 2007; Simons et al., 2010). Recent studies provided the possible *P-T* paths of various lithologies within the subducting slab beneath the district (Kimura et al., 2014; Syracuse et al., 2010), which allow us to precisely examine the change in elemental and isotopic compositions of subducted Li sources. The details about the modeling are given in Text S4.3 in Supporting Information S1, and the results are summarized in Tables S2 and S3 in Supporting Information S1. It is noted that subducted sediments would have incongruently melted, having left solid residues possibly containing Li-rich phases (e.g., garnet). Johnson and Plank (1999) analyzed [Li] of melts and residues produced by melting experiments of sedimentary starting materials. Their results do not show preferential retention of Li in residues ($[Li]_{residue}/[Li]_{starting\ material} < 1$ for all experiments). We thus consider that significant isotope fractionation did not occur during the formation of fluids or melts from subducted sediments.

Results of the modeling are shown in Figure 5 and Tables S2 and S3 in Supporting Information S1. The extents to which Li-isotope fractionation occur in AOC and SED largely depend on the amounts of fluids released from these lithologies. Then, the releases of fluids are governed by breakdowns of hydrous phases in AOC and SED. The models predicted that the [Li] and δ^7Li values of AOC and SED significantly decrease during subduction in the depth of >70 km (Figure 5). This is because major hydrous phases in AOC and SED (amphibole, lawsonite, chlorite, prehnite, pumpellyite, and talc) are broken down in these depths, as postulated by the model for SW Japan (Kimura, 2017; Kimura et al., 2014) using thermodynamic algorithms (Connolly & Kerrick, 1987; Connolly & Petrini, 2002). Nevertheless, the predicted changes of δ^7Li values to the depth for melting (90 km) are relatively small; 2‰ (+11.5‰ to +9.7‰) for AOC and 0.5‰ (−1.0‰ to −1.5‰) for SED, respectively. These changes accompany a significant decrease in Li abundances ($[Li]/[Li]_0$ = 56% for AOC and 27% for SED, respectively, where [Li] and $[Li]_0$ are Li abundances in subducted and pre-subducted AOC or SED, respectively).

5.4. Mantle Buffering of the Slab-Derived Li-Isotope Signature

The IAB magmas are considered to have been derived by partial melting of mantle metasomatized by slab-derived fluids or melts (Kimura et al., 2014; Nguyen et al., 2020). Most IAB rocks have δ^7Li values within the range of MORB. Slab-derived fluids would be a mixture of AOC- and SED-derived fluids or melts. The IAB source should have been heated to the temperature required for melting (1,220–1,380°C; Nguyen et al., 2020). Under such a high-temperature condition, the slab-derived Li-isotope signature may have been attenuated by diffusive isotope equilibrium with the mantle. The inference is supported by the homogeneity of δ^7Li values, falling within the range of unaltered MORB, in the majority of mantle-derived rocks distributed over the globe through geologic time (Halama et al., 2008; Krienitz et al., 2012).

Migration of slab-derived fluids or melts could have occurred in the form of (a) diffuse porous flow (Mibe et al., 1999), (b) fracture flow (Davies, 1999) or (c) diapir (Hall & Kincaid, 2001). Siliceous fluids or hydrous melts are highly viscous, resulting in low permeability. Thus, their transports likely occur in the form of either fracture flow (Kepezhinskas et al., 1996) or diapirs (Yogodzinski et al., 2015). Nevertheless, the likelihood of transport by diffuse porous flow is examined using the approach by Caciagli et al. (2011) using the chromatographic model of Navon and Stolper (1987). In the model, a mantle column consisting of mineral grains with

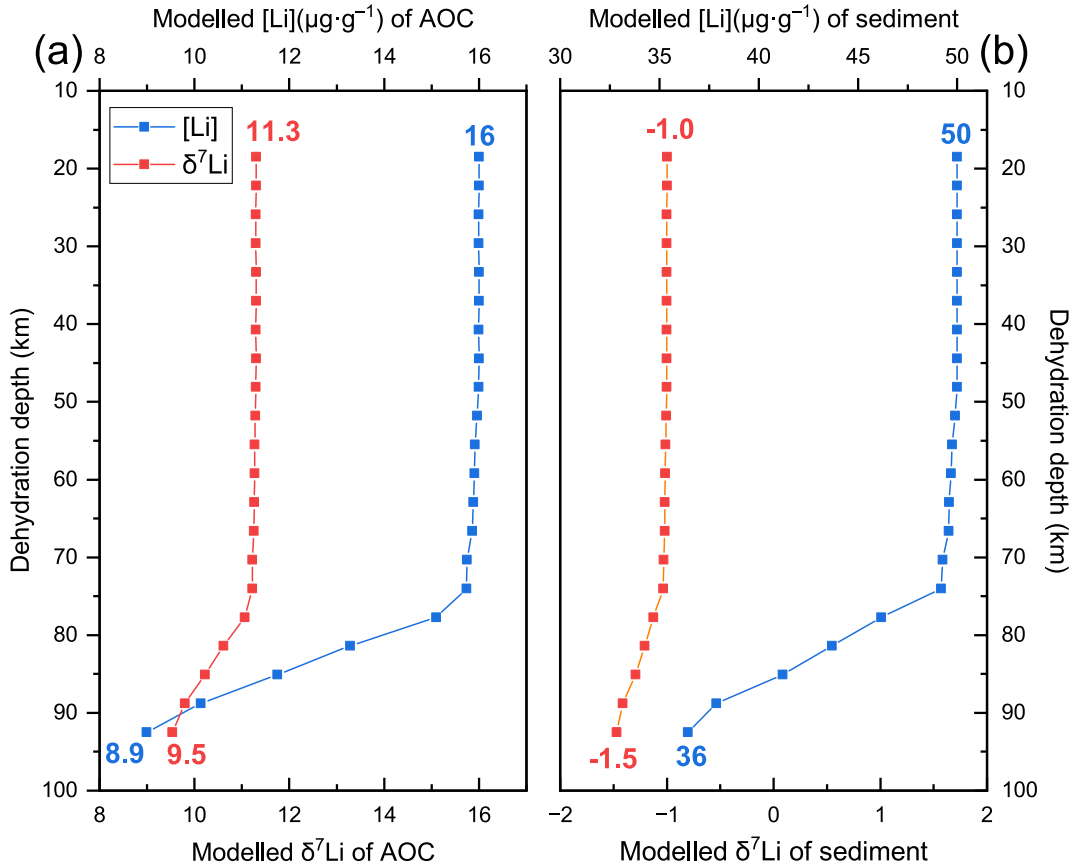

Figure 5. The changes in [Li] (blue lines) and δ^7Li values (red lines) of (a) altered oceanic crust (AOC) (Shikoku Basin basalt) and (b) sediment (Nankai sediment) in the subducted oceanic lithosphere at the depth from c. 20 to 90 km beneath the Chugoku district, calculated by the incremental dehydration model (H. R. Marschall et al., 2007; Simons et al., 2010). Significant drops in [Li] and δ^7Li values of AOC and sediment (SED) in the depth of >70 km are due to the breakdown of major hydrous phases in these materials (amphibole, lawsonite, chlorite, prehnite, pumpellyite, and talc).

interconnected pores is considered. Fluids or melts go upward through interconnected pore space in the mantle column of a finite length. The X_{melt} is the mass fraction of Li in the fluid/melt in the column defined as

$$X_{melt} \equiv \frac{\Phi\rho_{melt}}{\Phi\rho_{melt} + (1-\Phi)\rho_{mantle}K\mathrm{d}_{Li}} \quad (1)$$

where Φ is fluid/melt fraction in the mantle column (porosity), ρ_{melt} and ρ_{mantle} are the densities of a fluid/melt and the solid mantle, and $K\mathrm{d}_{Li}$ is partition coefficient of Li between the solid mantle and a fluid/melt ($K\mathrm{d}_{Li} \equiv [\mathrm{Li}]_{mantle}/[\mathrm{Li}]_{melt}$), respectively. The Φ of 0.03 follows Navon and Stolper (1987), and ρ_{melt} and ρ_{mantle} are assumed to be 3 and 3.25 g/cm^3 respectively (Jull & Kelemen, 2001; Pineda-Velasco et al., 2018). The K_d is estimated to be 0.25 from partitioning data for Li in mafic mineral phases (Adam & Green, 2006; Brenan et al., 1998; McDade et al., 2003; Ottolini et al., 2009) and the assumed mantle mineralogy (60 wt% olivine + 20 wt% clinopyroxene + 20 wt% orthopyroxene for fertile peridotite after McDonough and Rudnick (1998)). Further details are summarized in Text S5.1 in Supporting Information S1.

Using Equation 1, the mass fraction of Li retained in transported fluids/melts is estimated to be 10% ($X_{melt} = 0.1$). The mass fraction of Li is proportional to the velocity of Li in the mantle relative to the velocity of fluid/melt (Navon & Stolper, 1987); that is, Li moves 10 times slower than melt. Thus, the travel time of Li in the column is 10 times longer that the travel time of fluid/melt. The Daisen ADK samples have the (^{230}Th/^{232}Th) and (^{238}U/^{232}Th) activity ratios which indicate ^{238}U-^{230}Th disequilibrium (Feineman et al., 2013; Tokunaga et al., 2010). Given that the half-life of ^{230}Th (c. 75,000 years) and the melting depth (i.e., column length, c. 60 km; Pineda-Velasco

et al., 2018), the fluid/melt velocity is estimated to be c. 1 m·year^{-1}. Accordingly, the Li velocity is estimated to be c. 0.1 m·year^{-1} or 10 cm·year^{-1}. The base of the wedge mantle would have been dragged by the underlying slab due to mechanical coupling (Wada & Wang, 2009). Thus, a large quantity of Li could not migrate upward through the wedge mantle when the Li velocity is comparable to the slab descent rate. The slab descent rate in SW Japan is estimated to be 4.3 cm·year^{-1} (Syracuse et al., 2010), which is comparable to the Li velocity. Thus, transport of slab-derived Li by percolation of fluids through the mantle is unlikely.

The other feasible styles of melt transport are fracture flow or diapiric rise. The velocity of melts by these flow styles is more rapid. Also, the surface area to volume ratios of melts in these flow styles is significantly lower than that for porous flow. Thus, lesser extents of melt-mantle interaction are anticipated during melt migration (Navon & Stolper, 1987). Pineda-Velasco et al. (2018) argued that slab-derived melts were transported in the form of diapirs. In this case, Li isotope exchange occurs between a diapir and the surrounding mantle via diffusion at their contact. For modeling the change in Li isotope composition for this scenario, we applied the non-steady state radial diffusion model after Crank (1975) and Halama et al. (2008), expressed as

$$\frac{C - C_1}{C_0 - C_1} = 1 + \frac{2a}{\pi r}\sum_{n=1}^{\infty}\frac{(-1)^n}{n}\sin\frac{n\pi r}{a}\exp\left(\frac{-Dn^2\pi^2 t}{a^2}\right) \quad (2)$$

where C is [Li] at the distance r from the center of a spherical diapir (slab melt) with the radius a at time t, C_0 is the [Li] of the surface of a spherical diapir, C_1 is the initial [Li] (assumed to be homogeneous), D is the diffusion coefficient of Li, respectively. Note that r and a have the relationship of $0 \le r \le a$ or $0 \le r/a \le 1$. In the modeling, C_0 is [Li] of the mantle and C_1 is [Li] of the slab-derived melt.

The size of a diapir and the duration time of the diffusive reaction are essential input parameters for the modeling. The radius of a diapir is estimated to be 3–10 km from the size of each ADK volcano. The rising velocity is estimated to be 0.2–2 m·year^{-1} from the size and density of the diapir (Pineda-Velasco et al., 2018; this study). The travel time of diapir through the mantle is estimated to be 29,000–320,000 years (29–320 Kyrs). We assume that the travel time is the same as the duration time of a melt in the mantle. The details about the input parameters for modeling are present in Text S5.2 in Supporting Information S1.

The [Li] and δ^7Li variations at a given distance from the center of the diapir and a given temperature are shown in Figure 6. For a diapir >3 km in radius, the [Li] and δ^7Li values of a melt do not change significantly over the

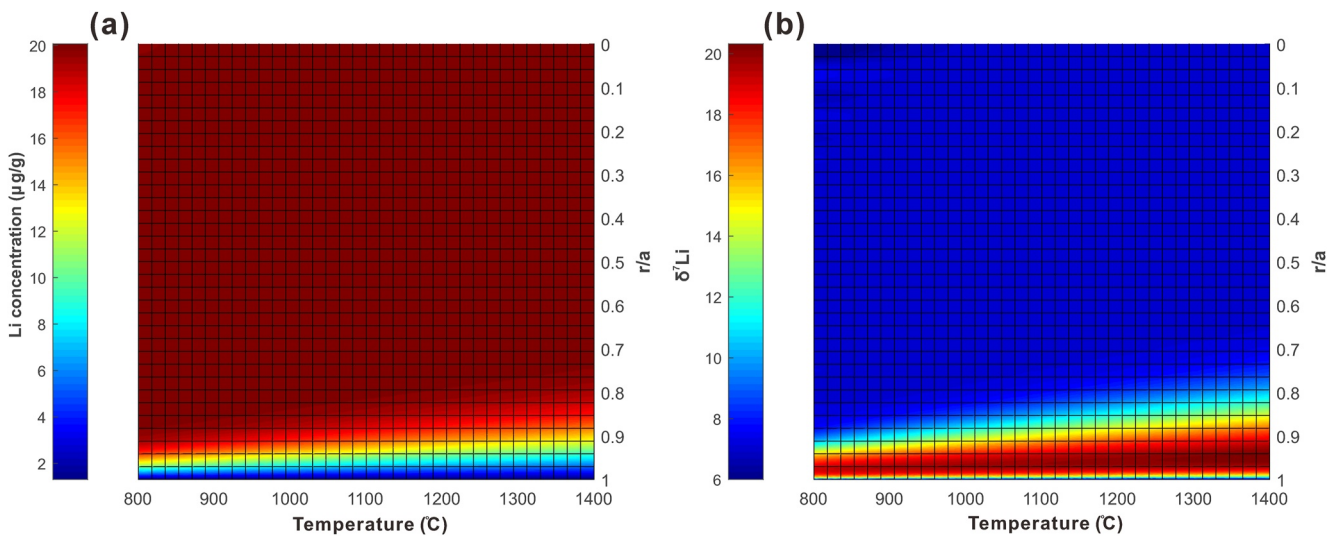

Figure 6. Diffusion modeling for temporal and spatial changes in (a) Li concentration ([Li]) and (b) δ^7Li values of a slab melt diapir with the radius of 3,000 m (initial [Li] = 20 µg·g^{-1} and initial δ^7Li = +7 ‰), having been preserved in the mantle ([Li] = 1.3 µg·g^{-1} and δ^7Li = +3.5‰) during 320 Kyrs. The changes in Li concentration and δ^7Li values in the diffusion surfaces are calculated across the distance from the surface to the center of a diapir and over the temperature range from 800°C (slab surface temperature at which slab melting occurred; Pineda-Velasco et al., 2018) to 1,400°C (maximum temperature of wedge mantle, estimated from primitive basalts; Nguyen et al., 2020). The *r/a* value is a dimensionless parameter based on the sphere's radius a and the distance from the sphere's center r, that is, the surface of the sphere corresponds to a value of 1.

time for transit (<320 Kyrs) through the mantle. The model well explains the preservation of high δ^7Li values in some ADK. The low-Mg character of most ADK samples also suggested that slab-derived melts did not reach Fe/Mg equilibrium with the mantle during their ascent to the surface (Pineda-Velasco et al., 2018).

An exception is for Aonoyama ADK samples all of which have the δ^7Li values (+1.6 to +3.3‰) well within the range of unaltered MORB. It should be noted that these ADK rocks (and IAB from the nearby region, Abu) plot off the arrays formed by the other ADK and IAB in Figure 3 to lower $^{87}Sr/^{86}Sr$ and $^{206}Pb/^{204}Pb$ and to higher $^{143}Nd/^{144}Nd$ and $^{176}Hf/^{177}Hf$. Pineda-Velasco et al. (2018) argued that the melting degree of AOC for Aonoyama ADK is smaller than that for the other ADK, while the melting degree of SED is similar among all ADK. Accordingly, the mixing occurs in higher $(Li/Sr)_{SED}/(Li/Sr)_{AOC}$, $(Li/Nd)_{SED}/(Li/Nd)_{AOC}$, $(Li/Hf)_{SED}/(Li/Hf)_{AOC}$ and $(Li/Pb)_{SED}/(Li/Pb)_{AOC}$ for Aonoyama ADK than those for other ADK (Text S6 and Figure S7 in Supporting Information S1). The obtained mixing relationships for Aonoyama and the other ADK are consistent with Feineman et al. (2013) and Pineda-Velasco et al. (2018).

5.5. Implications for Li Isotope Variation in Global Arc Magmas

Three scenarios have been proposed to explain the apparent similarity of δ^7Li values between island-arc rocks and MORB/mantle: (a) mixing of the mantle and subducted sediments, both of which have δ^7Li values indistinguishable from MORB (Plank, 2014; Tang et al., 2014), (b) contribution of the AOC-derived component with a MORB-like δ^7Li value by dehydration-induced isotopic fractionation (Leeman et al., 2004; Magna, Wiechert, Grove, et al., 2006), (c) buffering of slab-derived Li via diffusive isotopic exchange with surrounding mantle that has a MORB-like δ^7Li value (Caciagli et al., 2011; Halama et al., 2009; Tomascak et al., 2002). The feasibilities of these scenarios are examined using the results of this study.

The SW Japan arc provides a vital opportunity to examine Scenario 1, as the subducted sediments or the equivalents have δ^7Li values distinct from MORB (Moriguti & Nakamura, 1998; You et al., 1995) and yield magmas directly derived from sediments and AOC (Pineda-Velasco et al., 2018; Shimoda et al., 1998). We documented the Li-isotope compositions of these magmas akin to sediments or AOC. If AOC has the δ^7Li value significantly higher than unaltered MORB while sediments have the δ^7Li value significantly lower than unaltered MORB (or vice versa), then hybridization of these components can produce MORB-like δ^7Li values (Tomascak et al., 2016), as is found in SW Japan.

Scenario 2 requires the estimate of the extent to which Li isotopes fractionate during dehydration. SW Japan is an ideal field to examine the issue because the *P-T* path and metamorphic reaction of the subducting slab are well constrained (Kimura et al., 2014; van Keken et al., 2011) and the analysis of ADK offers us an opportunity to know the δ^7Li value of the subducted AOC after intensive dehydration (Feineman et al., 2013; Kimura et al., 2014; Pineda-Velasco et al., 2018). We demonstrated, based on numerical models, that Li isotopes fractionate to a limited extent, as proposed by H. R. Marschall et al. (2007), and it well explains the high δ^7Li values of ADK. Thus, Scenario 2 is unlikely for SW Japan and probably for many other arcs.

Scenario 3 can also be examined in SW Japan, as the arc yielded magmas that strongly reacted with the mantle (IAB and HMA). The effect of mantle buffering on Li isotope is inevitable, in particular, in the case of transport of fluids dominated by aqueous liquid (e.g., Caciagli et al., 2011; Halama et al., 2009; H. R. Marschall & Tang, 2020; Tomascak et al., 2002). In contrast, as our modeling suggested, if fluids are enriched in solute components, such as hydrous melt (ADK), they could move rapidly with larger masses in the forms of diapir (or fracture flow) and hence the slab-derived Li-isotope signature could be preserved. The scenario may explain the occurrence of volcanic rocks with higher-than-MORB δ^7Li values such as in the Cascades (Magna, Wiechert, Grove, et al., 2006) and lower-than-MORB δ^7Li values such as in the Lesser Antilles (Tang et al., 2014), where slab melt or sediment melt are proposed to be probable mechanisms to produce those arc magmas (Labanieh et al., 2012; Walowski et al., 2015, 2016).

Therefore, we suggest hybrid slab-derived components (from AOC and sediments), rather than subduction-induced dehydration or diffusive equilibrium with the mantle, would control the Li isotopic composition of arc magmas if the fluids/melts transport rapidly or voluminously, such as diapirs. Recent numerical models also predict the likelihood of incorporation of subducted materials as diapir (referred to as mélange diapir) into the wedge mantle (H. Marschall & Schumacher, 2012).

6. Conclusions

The main conclusions reached in this study are:

1. The late Cenozoic volcanic rocks in the Chugoku district show a large variation in δ^7Li values (−1.9 to +7.4 ‰), spanning beyond the entire range of MORB (+1.6 to +5.6 ‰), as a result of various extents of interaction among magma source components with different δ^7Li, derived from subducted sediments, subducted oceanic crust, and wedge mantle.
2. The lower-than-MORB δ^7Li values of high-Mg andesites and the higher-than-MORB δ^7Li values of high-Sr andesites and dacites (adakites) in the Chugoku district suggest large contributions of sediment and subducted basalts, respectively, to their magma sources.
3. Modeling the dehydration of subducted sediment (δ^7Li of −1‰) and oceanic crust (δ^7Li of +11 to +12‰) shows that δ^7Li values of these subducted materials were not significantly changed (<2‰) by metamorphic dehydration and could produce the variation in δ^7Li values in the mantle beneath the district.
4. Modeling the diffusive isotope equilibrium indicates that the transport of melts from subducted sediments or oceanic crusts was fast (~1 m·year^{-1}) enough to retain the δ^7Li values of when they were formed, and suggests the possible melt transport mechanism of diapiric rise or fracture flow.

Data Availability Statement

All data used for this research are available in the Supporting Information S1 and can be found online (https://figshare.com/articles/figure/Supporting_Information_for_Lithium_isotope_constraints_on_slab_and_mantle_contribution_to_arc_magmas_/21195844).

Acknowledgments
The authors would like to thank members of the Pheasant Memorial Laboratory for the support in the laboratory for helpful discussions and Tatsumi Yoshiyuki for the donation of the samples of Setouchi HMA. We also thank C. Potiszil for improving the initial manuscript. We are grateful to two anonymous reviewers and Fang-Zhen Teng for their careful and constructive comments and Mark Dekkers for the editorial handling. Financial support for this project was provided by the Program for Promoting the Enhancement of Research University by MEXT and JST SPRING (Grant Number JPMJSP2126, Japan).

References

Abers, G. A., van Keken, P. E., & Hacker, B. R. (2017). The cold and relatively dry nature of mantle forearcs in subduction zones. *Nature Geoscience*, *10*(5), 333–337. https://doi.org/10.1038/ngeo2922

Adam, J., & Green, T. (2006). Trace element partitioning between mica-and amphibole-bearing garnet lherzolite and hydrous basanitic melt: 1. Experimental results and the investigation of controls on partitioning behaviour. *Contributions to Mineralogy and Petrology*, *152*(1), 1–17. https://doi.org/10.1007/s00410-006-0085-4

Agostini, S., Ryan, J. G., Tonarini, S., & Innocenti, F. (2008). Drying and dying of a subducted slab: Coupled Li and B isotope variations in Western Anatolia Cenozoic Volcanism. *Earth and Planetary Science Letters*, *272*(1–2), 139–147. https://doi.org/10.1016/j.epsl.2008.04.032

Asamori, K., & Zhao, D. (2015). Teleseismic shear wave tomography of the Japan subduction zone. *Geophysical Journal International*, *203*(3), 1752–1772. https://doi.org/10.1093/gji/ggv334

Babechuk, M. G., Widdowson, M., & Kamber, B. S. (2014). Quantifying chemical weathering intensity and trace element release from two contrasting basalt profiles, Deccan Traps, India. *Chemical Geology*, *363*, 56–75. https://doi.org/10.1016/j.chemgeo.2013.10.027

Berger, G., Schott, J., & Guy, C. (1988). Behavior of Li, Rb and Cs during basalt glass and olivine dissolution and chlorite, smectite and zeolite precipitation from seawater: Experimental investigations and modelization between 50 and 300°C. *Chemical Geology*, *71*(4), 297–312. https://doi.org/10.1016/0009-2541(88)90056-3

Bouman, C., Elliott, T., & Vroon, P. Z. (2004). Lithium inputs to subduction zones. *Chemical Geology*, *212*(1–2), 59–79. https://doi.org/10.1016/j.chemgeo.2004.08.004

Brant, C., Coogan, L. A., Gillis, K. M., Seyfried, W. E., Pester, N. J., & Spence, J. (2012). Lithium and Li-isotopes in young altered upper oceanic crust from the East Pacific Rise. *Geochimica et Cosmochimica Acta*, *96*, 272–293. https://doi.org/10.1016/j.gca.2012.08.025

Brenan, J. M., Ryerson, F. J., & Shaw, H. F. (1998). The role of aqueous fluids in the slab-to-mantle transfer of boron, beryllium, and lithium during subduction; experiments and models. *Geochimica et Cosmochimica Acta*, *62*(19–20), 3337–3347. https://doi.org/10.1016/S0016-7037(98)00224-5

Brens, R., Jr., Liu, X. M., Turner, S., & Rushmer, T. (2019). Lithium isotope variations in Tonga–Kermadec arc–Lau back-arc lavas and Deep Sea Drilling Project (DSDP) Site 204 sediments. *Island Arc*, *28*(1). https://doi.org/10.1111/iar.12276

Caciagli, N., Brenan, J. M., McDonough, W. F., & Phinney, D. (2011). Mineral–fluid partitioning of lithium and implications for slab–mantle interaction. *Chemical Geology*, *280*(3–4), 384–398. https://doi.org/10.1016/j.chemgeo.2010.11.025

Chan, L. H., Leeman, W. P., & Plank, T. (2006). Lithium isotopic composition of marine sediments. *Geochemistry, Geophysics, Geosystems*, *7*(6), Q06005. https://doi.org/10.1029/2005GC001202

Chan, L. H., Leeman, W. P., & You, C. F. (2002). Lithium isotopic composition of Central American volcanic arc lavas: Implications for modification of subarc mantle by slab-derived fluids: Correction. *Chemical Geology*, *182*(2), 293–300. https://doi.org/10.1016/S0009-2541(01)00298-4

Connolly, J. A. D., & Kerrick, D. M. (1987). An algorithm and computer program for calculating composition phase diagrams. *Calphad*, *11*(1), 1–55. https://doi.org/10.1016/0364-5916(87)90018-6

Connolly, J. A. D., & Petrini, K. (2002). An automated strategy for calculation of phase diagram sections and retrieval of rock properties as a function of physical conditions. *Journal of Metamorphic Geology*, *20*(7), 697–708. https://doi.org/10.1046/j.1525-1314.2002.00398.x

Crank, J. (1975). *The mathematics of diffusion* (2nd ed.). Clarendon Press.

Davies, J. H. (1999). The role of hydraulic fractures and intermediate-depth earthquakes in generating subduction-zone magmatism. *Nature*, *398*(6723), 142–145. https://doi.org/10.1038/18202

Decitre, S., Deloule, E., Reisberg, L., James, R., Agrinier, P., & Mével, C. (2002). Behavior of Li and its isotopes during serpentinization of oceanic peridotites. *Geochemistry, Geophysics, Geosystems*, *3*(1), 1–20. https://doi.org/10.1029/2001GC000178

Dohmen, R., Kasemann, S. A., Coogan, L., & Chakraborty, S. (2010). Diffusion of Li in olivine. Part I: Experimental observations and a multi species diffusion model. *Geochimica et Cosmochimica Acta*, *74*(1), 274–292. https://doi.org/10.1016/j.gca.2009.10.016

Feineman, M., Moriguti, T., Yokoyama, T., Terui, S., & Nakamura, E. (2013). Sediment-enriched adakitic magmas from the Daisen volcanic field, Southwest Japan. *Geochemistry, Geophysics, Geosystems*, *14*(8), 3009–3031. https://doi.org/10.1002/ggge.20176

Halama, R., McDonough, W. F., Rudnick, R. L., & Bell, K. (2008). Tracking the lithium isotopic evolution of the mantle using carbonatites. *Earth and Planetary Science Letters*, *265*(3–4), 726–742. https://doi.org/10.1016/j.epsl.2007.11.007

Halama, R., Savov, I. P., Rudnick, R. L., & McDonough, W. F. (2009). Insights into Li and Li isotope cycling and sub-arc metasomatism from veined mantle xenoliths, Kamchatka. *Contributions to Mineralogy and Petrology*, *158*(2), 197–222. https://doi.org/10.1007/s00410-009-0378-5

Hall, P. S., & Kincaid, C. (2001). Diapiric flow at subduction zones: A recipe for rapid transport. *Science*, *292*(5526), 2472–2475. https://doi.org/10.1126/science.106048

Hanna, H. D., Liu, X., Park, Y., Kay, S. M., & Rudnick, R. L. (2020). Lithium isotopes may trace subducting slab signatures in Aleutian arc lavas and intrusions. *Geochimica et Cosmochimica Acta*, *278*, 322–339. https://doi.org/10.1016/j.gca.2019.07.049

Hanyu, T., Tatsumi, Y., & Nakai, S. (2002). A contribution of slab-melts to the formation of high-Mg andesite magmas; Hf isotopic evidence from SW Japan. *Geophysical Research Letters*, *29*(22), 1–8. https://doi.org/10.1029/2002GL015856

Hickey-Vargas, R. (1991). Isotope characteristics of submarine lavas from the Philippine Sea: Implications for the origin of arc and basin magmas of the Philippine tectonic plate. *Earth and Planetary Science Letters*, *107*(2), 290–304. https://doi.org/10.1016/0012-821X(91)90077-U

Hickey-Vargas, R. (1998). Origin of the Indian Ocean-type isotopic signature in basalts from Philippine Sea plate spreading centers: An assessment of local versus large-scale processes. *Journal of Geophysical Research*, *103*(B9), 20963–20979. https://doi.org/10.1029/98JB02052

Imai, N., Terashima, S., Itoh, S., & Ando, A. (1995). 1994 compilation values for GSJ reference samples, "Igneous rock series". *Geochemical Journal*, *29*(1), 91–95. https://doi.org/10.2343/geochemj.29.91

Ishihara, S., & Tani, K. (2013). Zircon age of granitoids hosting molybdenite-quartz vein deposits in the central Sanin Belt, Southwest Japan. *Shigen-Chishitsu*, *63*(1), 11–14. https://doi.org/10.11456/shigenchishitsu.63.11

Ishikawa, T., & Nakamura, E. (1994). Origin of the slab component in arc lavas from across-arc variation of B and Pb isotopes. *Nature*, *370*(6486), 205–208. https://doi.org/10.1038/370205a0

Ishizaka, K., & Carlson, R. W. (1983). Nd-Sr systematics of the Setouchi volcanic rocks, southwest Japan: A clue to the origin of orogenic andesite. *Earth and Planetary Science Letters*, *64*(3), 327–340. https://doi.org/10.1016/0012-821X(83)90094-8

Ishizuka, O., Yuasa, M., Taylor, R. N., & Sakamoto, I. (2009). Two contrasting magmatic types coexist after the cessation of back-arc spreading. *Chemical Geology*, *266*(3–4), 274–296. https://doi.org/10.1016/j.chemgeo.2009.06.014

Iwamori, H. (1991). Zonal structure of Cenozoic basalts related to mantle upwelling in southwest Japan. *Journal of Geophysical Research*, *96*(B4), 6157–6170. https://doi.org/10.1029/90JB02399

Japan Meteorological Agency. (2013). In Japan Meteorological Agency and Volcanological Society of Japan (Ed.) *National catalogue of the active volcanoes in Japan* (4th ed.). Japan Meteorological Agency. Retrieved from https://www.data.jma.go.jp/vois/data/tokyo/STOCK/souran_eng/menu.htm

Jeffcoate, A. B., Elliott, T., Kasemann, S. A., Ionov, D., Cooper, K., & Brooker, R. (2007). Li isotope fractionation in peridotites and mafic melts. *Geochimica et Cosmochimica Acta*, *71*(1), 202–218. https://doi.org/10.1111/j.1751-908X.2004.tb01053.x

Johnson, M. C., & Plank, T. (1999). Dehydration and melting experiments constrain the fate of subducted sediments. *Geochemistry, Geophysics, Geosystems*, *1*(12), 1007. https://doi.org/10.1029/1999GC000014

Jull, M., & Kelemen, P. B. (2001). On the conditions for lower crustal convective instability. *Journal of Geophysical Research*, *106*(B4), 6423–6446. https://doi.org/10.1029/2000JB900357

Kawamoto, T., Kanzaki, M., Mibe, K., Matsukage, K. N., & Ono, S. (2012). Separation of supercritical slab-fluids to form aqueous fluid and melt components in subduction zone magmatism. *Proceedings of the National Academy of Sciences*, *109*(46), 18695–18700. https://doi.org/10.1073/pnas.1207687109

Kepezhinskas, P., Defant, M. J., & Drummond, M. S. (1996). Progressive enrichment of island arc mantle by melt-peridotite interaction inferred from Kamchatka xenoliths. *Geochimica et Cosmochimica Acta*, *60*(7), 1217–1229. https://doi.org/10.1016/0016-7037(96)00001-4

Kessel, R., Schmidt, M. W., Ulmer, P., & Pettke, T. (2005). Trace element signature of subduction-zone fluids, melts and supercritical liquids at 120–180 km depth. *Nature*, *437*(7059), 724–727. https://doi.org/10.1038/nature03971

Kimura, J.-I. (2017). Modeling chemical geodynamics of subduction zones using the Arc Basalt Simulator version 5. *Geosphere*, *13*(4), 992–1025. https://doi.org/10.1130/GES01468.1

Kimura, J.-I., Gill, J. B., Kunikiyo, T., Osaka, I., Shimoshioiri, Y., Katakuse, M., et al. (2014). Diverse magmatic effects of subducting a hot slab in SW Japan: Results from forward modeling. *Geochemistry, Geophysics, Geosystems*, *15*(3), 691–739. https://doi.org/10.1002/2013GC005132

Kimura, J.-I., Stern, R. J., & Yoshida, T. (2005). Reinitiation of subduction and magmatic responses in SW Japan during Neogene time. *Geological Society of America Bulletin*, *117*(7–8), 969–986. https://doi.org/10.1130/B25565.1

Kobayashi, K., Tanaka, R., Moriguti, T., Shimizu, K., & Nakamura, E. (2004). Lithium, boron, and lead isotope systematics of glass inclusions in olivines from Hawaiian lavas: Evidence for recycled components in the Hawaiian plume. *Chemical Geology*, *212*(1–2), 143–161. https://doi.org/10.1016/j.chemgeo.2004.08.050

Košler, J., Magna, T., Mlčoch, B., Mixa, P., Nývlt, D., & Holub, F. V. (2009). Combined Sr, Nd, Pb and Li isotope geochemistry of alkaline lavas from northern James Ross Island (Antarctic Peninsula) and implications for back-arc magma formation. *Chemical Geology*, *258*(3–4), 207–218. https://doi.org/10.1016/j.chemgeo.2008.10.006

Krienitz, M.-S., Garbe-Schönberg, C.-D., Romer, R. L., Meixner, A., Haase, K. M., & Stroncik, N. A. (2012). Lithium isotope variations in ocean island basalts—Implications for the development of mantle heterogeneity. *Journal of Petrology*, *53*(11), 2333–2347. https://doi.org/10.1093/petrology/egs052

Labanieh, S., Chauvel, C., Germa, A., & Quidelleur, X. (2012). Martinique: A clear case for sediment melting and slab dehydration as a function of distance to the trench. *Journal of Petrology*, *53*(12), 2441–2464. https://doi.org/10.1093/petrology/egs055

Lai, Y. J., Pogge von Strandmann, P. A. E., Dohmen, R., Takazawa, E., & Elliott, T. (2015). The influence of melt infiltration on the Li and Mg isotopic composition of the Horoman Peridotite Massif. *Geochimica et Cosmochimica Acta*, *164*, 318–332. https://doi.org/10.1016/j.gca.2015.05.006

Langmuir, C. H., Klein, E. M., & Plank, T. (1992). Petrological systematics of mid-ocean ridge basalts: Constraints on melt generation beneath ocean ridges. In J. Phipps Morgan, D. K. Blackman, & J. M. Sinton (Eds.), *Mantle flow and melt generation at mid-ocean ridges* (pp. 183–280). American Geophysical Union. https://doi.org/10.1029/GM071p0183

Leeman, W. P., Tonarini, S., Chan, L. H., & Borg, L. E. (2004). Boron and lithium isotopic variations in a hot subduction zone—The southern Washington Cascades. *Chemical Geology*, *212*(1–2), 101–124. https://doi.org/10.1016/j.chemgeo.2004.08.010

Liu, H., Xiao, Y., Sun, H., Tong, F., Heuser, A., Churikova, T., & Wörner, G. (2020). Trace elements and Li isotope compositions across the Kamchatka Arc: Constraints on slab-derived fluid sources. *Journal of Geophysical Research: Solid Earth*, *125*(5), e2019JB019237. https://doi.org/10.1029/2019JB019237

Magna, T., Janoušek, V., Kohút, M., Oberli, F., & Wiechert, U. (2010). Fingerprinting sources of orogenic plutonic rocks from Variscan belt with lithium isotopes and possible link to subduction-related origin of some A-type granites. *Chemical Geology*, *274*(1–2), 94–107. https://doi.org/10.1016/j.chemgeo.2010.03.020

Magna, T., Wiechert, U., Grove, T. L., & Halliday, A. N. (2006). Lithium isotope fractionation in the southern Cascadia subduction zone. *Earth and Planetary Science Letters*, *250*(3–4), 428–443. https://doi.org/10.1016/j.epsl.2006.08.019

Magna, T., Wiechert, U., & Halliday, A. N. (2006). New constraints on the lithium isotope compositions of the Moon and terrestrial planets. *Earth and Planetary Science Letters*, *243*(3–4), 336–353. https://doi.org/10.1016/j.epsl.2006.01.005

Mahony, S. H., Wallace, L. M., Miyoshi, M., Villamor, P., Sparks, R. S. J., & Hasenaka, T. (2011). Volcano-tectonic interactions during rapid plate-boundary evolution in the Kyushu region, SW Japan. *Geological Society of America Bulletin*, *123*(11–12), 2201–2223. https://doi.org/10.1130/B30408.1

Marschall, H., & Schumacher, J. (2012). Arc magmas sourced from mélange diapirs in subduction zones. *Nature Geoscience*, *5*(12), 862–867. https://doi.org/10.1038/ngeo1634

Marschall, H. R., Pogge von Strandmann, P. A. E., Seitz, H., Elliott, T., & Niu, Y. (2007). The lithium isotopic composition of orogenic eclogites and deep subducted slabs. *Earth and Planetary Science Letters*, *262*(3–4), 563–580. https://doi.org/10.1016/j.epsl.2007.08.005

Marschall, H. R., & Tang, M. (2020). High-temperature processes; is it time for lithium isotopes? *Elements (Quebec)*, *16*(4), 247–252. https://doi.org/10.2138/gselements.16.4.247

Marschall, H. R., Wanless, V. D., Shimizu, N., Pogge von Strandmann, P. A. E., Elliott, T., & Monteleone, B. D. (2017). The boron and lithium isotopic composition of mid-ocean ridge basalts and the mantle. *Geochimica et Cosmochimica Acta*, *207*, 102–138. https://doi.org/10.1016/j.gca.2017.03.028

McDade, P., Blundy, J. D., & Wood, B. J. (2003). Trace element partitioning on the Tinaquillo Lherzolite solidus at 1.5 GPa. *Physics of the Earth and Planetary Interiors*, *139*(1–2), 129–147. https://doi.org/10.1016/S0031-9201(03)00149-3

McDonough, W. F., & Rudnick, R. L. (1998). Mineralogy and composition of the upper mantle. *Reviews in Mineralogy*, *37*, 139–164. https://doi.org/10.1029/GL011i007p00637

McLennan, S. M. (1993). Weathering and global denudation. *The Journal of Geology*, *101*(2), 295–303. https://doi.org/10.1086/648222

Mibe, K., Fujii, T., & Yasuda, A. (1999). Control of the location of the volcanic front in island arcs by aqueous fluid connectivity in the mantle wedge. *Nature*, *401*(6750), 259–262. https://doi.org/10.1038/45762

Moore, G. F., Taira, A., Klaus, A., Becker, L., Boeckel, B., Cragg, B. A., et al. (2001). New insights into deformation and fluid flow processes in the Nankai Trough accretionary prism: Results of Ocean Drilling Program Leg 190. *Geochemistry, Geophysics, Geosystems*, *2*(10), 1058. https://doi.org/10.1029/2001GC000166

Moriguti, T., & Nakamura, E. (1998). Across-arc variation of Li isotopes in lavas and implications for crust/mantle recycling at subduction zones. *Earth and Planetary Science Letters*, *163*(1), 167–174. https://doi.org/10.1016/S0012-821X(98)00184-8

Moriguti, T., Shibata, T., & Nakamura, E. (2004). Lithium, boron and lead isotope and trace element systematics of Quaternary basaltic volcanic rocks in northeastern Japan: Mineralogical controls on slab-derived fluid composition. *Chemical Geology*, *212*(1–2), 81–100. https://doi.org/10.1016/j.chemgeo.2004.08.005

Nakamura, E., Campbell, I. H., & Sun, S.-s. (1985). The influence of subduction processes on the geochemistry of Japanese alkaline basalts. *Nature*, *316*(6023), 55–58. https://doi.org/10.1038/316055a0

Nakamura, E., Makishima, A., Moriguti, T., Kobayashi, K., Sakaguchi, C., Yokoyama, T., et al. (2003). Comprehensive geochemical analyses of small amounts (<100 mg) of extraterrestrial samples for the analytical competition related to the sample return mission MUSES-C. *The Institute of Space and Astronautical Science Report S.P.*, *16*, 49–101.

Navon, O., & Stolper, E. (1987). Geochemical consequences of melt percolation: The upper mantle as a chromatographic column. *The Journal of Geology*, *95*(3), 285–307. https://doi.org/10.1086/629131

Nesbitt, H. W., & Young, G. M. (1982). Early Proterozoic climates and plate motions inferred from major element chemistry of lutites. *Nature*, *299*(5885), 715–717. https://doi.org/10.1038/299715a0

Neukampf, J., Laurent, O., Tollan, P., Bouvier, A., Magna, T., Ulmer, P., et al. (2022). Degassing from magma reservoir to eruption in silicic systems: The Li elemental and isotopic record from rhyolitic melt inclusions and host quartz in a Yellowstone rhyolite. *Geochimica et Cosmochimica Acta*, *326*, 56–76. https://doi.org/10.1016/j.gca.2022.03.037

Nguyen, T. T., Kitagawa, H., Pineda Velasco, I., & Nakamura, E. (2020). Feedback of slab distortion on volcanic arc evolution: Geochemical perspective from late Cenozoic volcanism in SW Japan. *Journal of Geophysical Research: Solid Earth*, *125*(10), e2019JB019143. https://doi.org/10.1029/2019JB019143

Noguchi, M., Kamei, A., Suzuki, H., & Kobayashi, N. (2021). Igneous activity of the Daito granodiorite in Un-nan area, San'in zone, Southwest Japan. *Journal of Geological Society of Japan*, *127*(8), 461–478. https://doi.org/10.5575/geosoc.2021.0016

Oi, T., Odagiri, T., & Nomura, M. (1997). Extraction of lithium from GSJ rock reference samples and determination of their lithium isotopic compositions. *Analytica Chimica Acta*, *340*(1–3), 221–225. https://doi.org/10.1016/S0003-2670(96)00519-3

Ottolini, L., Laporte, D., Raffone, N., Devidal, J., & Le Fèvre, B. (2009). New experimental determination of Li and B partition coefficients during upper mantle partial melting. *Contributions to Mineralogy and Petrology*, *157*(3), 313–325. https://doi.org/10.1007/s00410-008-0336-7

Palmer, M. R., & Edmond, J. M. (1989). Cesium and rubidium in submarine hydrothermal fluids: Evidence for recycling of alkali elements. *Earth and Planetary Science Letters*, *95*(1–2), 8–14. https://doi.org/10.1016/0012-821X(89)90163-5

Parkinson, I., Hammond, S., James, R., & Rogers, N. (2007). High-temperature lithium isotope fractionation: Insights from lithium isotope diffusion in magmatic systems. *Earth and Planetary Science Letters*, *257*(3–4), 609–621. https://doi.org/10.1016/j.epsl.2007.03.023

Peacock, S. M., & Wang, K. (1999). Seismic consequences of warm versus cool subduction metamorphism: Examples from Southwest and Northeast Japan. *Science*, *286*(5441), 937–939. https://doi.org/10.1126/science.286.5441.937

Penniston-Dorland, S., Liu, X.-M., & Rudnick, R. L. (2017). Lithium isotope geochemistry. *Reviews in Mineralogy and Geochemistry*, *82*(1), 165–217. https://doi.org/10.2138/rmg.2017.82.6

Perfit, M. R., Gust, D. A., Bence, A. E., Arculus, R. J., & Taylor, S. R. (1980). Chemical characteristics of island-arc basalts: Implications for mantle sources. *Chemical Geology*, *30*(3), 227–256. https://doi.org/10.1016/0009-2541(80)90107-2

Pineda-Velasco, I., Kitagawa, H., Nguyen, T. T., Kobayashi, K., & Nakamura, E. (2018). Production of high-Sr andesite and dacite magmas by melting of subducting oceanic lithosphere at propagating slab tears. *Journal of Geophysical Research: Solid Earth*, *123*(5), 3698–3728. https://doi.org/10.1029/2017JB015066

Plank, T. (2014). The chemical composition of subducting sediments. In R. L. Rudnick (Ed.), *The crust. Treatise on Geochemistry* (2nd ed., Vol. 4, pp. 607–629. H. D. Holland, & K. K. Turekian (Eds.)). Elsevier Ltd. https://doi.org/10.1016/B978-0-08-095975-7.00319-3

Plank, T., & Langmuir, C. H. (1998). The chemical composition of subducting sediment and its consequences for the crust and mantle. *Chemical Geology*, *145*(3–4), 325–394. https://doi.org/10.1016/S0009-2541(97)00150-2

Pogge von Strandmann, P. A. E., Elliott, T., Marschall, H. R., Coath, C., Lai, Y.-J., Jeffcoate, A. B., & Ionov, D. A. (2011). Variations of Li and Mg isotope ratios in bulk chondrites and mantle xenoliths. *Geochimica et Cosmochimica Acta*, *75*(18), 5247–5268. https://doi.org/10.1016/j.gca.2011.06.026

Sakuyama, M., & Nesbitt, R. W. (1986). Geochemistry of the Quaternary volcanic rocks of the northeast Japan arc. *Journal of Volcanology and Geothermal Research*, *29*(1–4), 413–450. https://doi.org/10.1016/0377-0273(86)90053-3

Scambelluri, M., Müntener, O., Ottolini, L., Pettke, T. T., & Vannucci, R. (2004). The fate of B, Cl and Li in the subducted oceanic mantle and in the antigorite breakdown fluids. *Earth and Planetary Science Letters*, *222*(1), 217–234. https://doi.org/10.1016/j.epsl.2004.02.012

Schiavi, F., Kobayashi, K., Moriguti, T., Nakamura, E., Pompilio, M., Tiepolo, M., & Vannucci, R. (2010). Degassing, crystallization and eruption dynamics at Stromboli: Trace element and lithium isotopic evidence from 2003 ashes. *Contributions to Mineralogy and Petrology*, *159*(4), 541–561. https://doi.org/10.1007/s00410-009-0441-2

Schiavi, F., Kobayashi, K., Nakamura, E., Tiepolo, M., & Vannucci, R. (2012). Trace element and Pb–B–Li isotope systematics of olivine-hosted melt inclusions: Insights into source metasomatism beneath Stromboli (southern Italy). *Contributions to Mineralogy and Petrology*, *163*(6), 1011–1031. https://doi.org/10.1007/s00410-011-0713-5

Schuessler, J. A., Schoenberg, R., & Sigmarsson, O. (2009). Iron and lithium isotope systematics of the Hekla volcano, Iceland—Evidence for Fe isotope fractionation during magma differentiation. *Chemical Geology*, *258*(1–2), 78–91. https://doi.org/10.1016/j.chemgeo.2008.06.021

Seitz, H. M., Brey, G. P., Lahaye, Y., Durali, S., & Weyer, S. (2004). Lithium isotopic signatures of peridotite xenoliths and isotopic fractionation at high temperature between olivine and pyroxenes. *Chemical Geology*, *212*(1–2), 163–177. https://doi.org/10.1016/j.chemgeo.2004.08.009

Seyfried, W. E., Jr., Chen, X., & Chan, L. (1998). Trace element mobility and lithium isotope exchange during hydrothermal alteration of seafloor weathered basalt: An experimental study at 350°C, 500 bars. *Geochimica et Cosmochimica Acta*, *62*(6), 949–960. https://doi.org/10.1016/S0016-7037(98)00045-3

Shibata, T., & Nakamura, E. (1997). Across-arc variations of isotope and trace element compositions from Quaternary basaltic volcanic rocks in northeastern Japan: Implications for interaction between subducted oceanic slab and mantle wedge. *Journal of Geophysical Research*, *102*(B4), 8051–8064. https://doi.org/10.1029/96JB03661

Shimoda, G., Tatsumi, Y., Nohda, S., Ishizaka, K., & Jahn, B. M. (1998). Setouchi high-Mg andesites revisited: Geochemical evidence for melting of subducting sediments. *Earth and Planetary Science Letters*, *160*(3–4), 479–492. https://doi.org/10.1016/S0012-821X(98)00105-8

Shu, Y., Nielsen, S. G., Zeng, Z., Shinjo, R., Blusztajn, J., Wang, X., & Chen, S. (2017). Tracing subducted sediment inputs to the Ryukyu arc-Okinawa Trough system: Evidence from thallium isotopes. *Geochimica et Cosmochimica Acta*, *217*, 462–491. https://doi.org/10.1016/j.gca.2017.08.035

Simons, K. K., Harlow, G. E., Brueckner, H. K., Goldstein, S. L., Sorensen, S. S., Hemming, N. G., & Langmuir, C. H. (2010). Lithium isotopes in Guatemalan and Franciscan HP–LT rocks: Insights into the role of sediment-derived fluids during subduction. *Geochimica et Cosmochimica Acta*, *74*(12), 3621–3641. https://doi.org/10.1016/j.gca.2010.02.033

Straub, S. M., Goldstein, S. L., Class, C., Schmidt, A., & Gomez-Tuena, A. (2010). Slab and mantle controls on the Sr–Nd–Pb–Hf isotope evolution of the post 42 Ma Izu–Bonin Volcanic Arc. *Journal of Petrology*, *51*(5), 993–1026. https://doi.org/10.1093/petrology/egq009

Syracuse, E. M., & Abers, G. A. (2006). Global compilation of variations in slab depth beneath arc volcanoes and implications. *Geochemistry, Geophysics, Geosystems*, *7*(5), Q05017. https://doi.org/10.1029/2005GC001045

Syracuse, E. M., van Keken, P. E., & Abers, G. A. (2010). The global range of subduction zone thermal models. *Physics of the Earth and Planetary Interiors*, *183*(1–2), 73–90. https://doi.org/10.1016/j.pepi.2010.02.004

Taira, A., Katto, J., Tashiro, M., Okamura, M., & Kodama, K. (1988). The Shimanto Belt in Shikoku, Japan–Evolution of Cretaceous to Miocene accretionary prism. *Modern Geology*, *12*, 5–46.

Tang, M., Rudnick, R. L., & Chauvel, C. (2014). Sedimentary input to the source of Lesser Antilles lavas: A Li perspective. *Geochimica et Cosmochimica Acta*, *144*, 43–58. https://doi.org/10.1016/j.gca.2014.09.003

Tatsumi, Y., & Hanyu, T. (2003). Geochemical modeling of dehydration and partial melting of subducting lithosphere: Toward a comprehensive understanding of high-Mg andesite formation in the Setouchi volcanic belt, SW Japan. *Geochemistry, Geophysics, Geosystems*, *4*(1081), 1081. https://doi.org/10.1029/2003GC000530

Tatsumi, Y., & Ishizaka, K. (1982a). Origin of high-magnesian andesites in the Setouchi volcanic belt, southwest Japan, I. Petrographical and chemical characteristics. *Earth and Planetary Science Letters*, *60*(2), 293–304. https://doi.org/10.1016/0012-821X(82)90008-5

Tatsumi, Y., & Ishizaka, K. (1982b). Magnesian andesite and basalt from Shodo-Shima Island, southwest Japan, and their bearing on the genesis of calc-alkaline andesites. *Lithos*, *15*(2), 161–172. https://doi.org/10.1016/0024-4937(82)90007-X

Tatsumi, Y., Suenaga, N., Yoshioka, S., Kaneko, K., & Matsumoto, T. (2020). Contrasting volcano spacing along SW Japan arc caused by difference in age of subducting lithosphere. *Scientific Reports*, *10*(1), 15005. https://doi.org/10.1038/s41598-020-72173-6

Terakado, Y., Shimizu, H., & Masuda, A. (1988). Nd and Sr isotopic variations in acidic rocks formed under a peculiar tectonic environment in Miocene Southwest Japan. *Contributions to Mineralogy and Petrology*, *99*(1), 1–10. https://doi.org/10.1007/BF00399360

Tokunaga, S., Nakai, S., & Orihashi, Y. (2010). Two types of adakites revealed by ^{238}U-^{230}Th disequilibrium from Daisen Volcano, southwestern Japan. *Geochemical Journal*, *44*(5), 379–386. https://doi.org/10.2343/geochemj.1.0080

Tomascak, P. B., Langmuir, C. H., le Roux, P. J., & Shirey, S. B. (2008). Lithium isotopes in global mid-ocean ridge basalts. *Geochimica et Cosmochimica Acta*, *72*(6), 1626–1637. https://doi.org/10.1016/j.gca.2007.12.021

Tomascak, P. B., Magna, T., & Dohmen, R. (2016). *Advances in lithium isotope geochemistry*. Springer Cham. https://doi.org/10.1007/978-3-319-01430-2

Tomascak, P. B., Ryan, J. G., & Defant, M. J. (2000). Lithium isotope evidence for light element decoupling in the Panama subarc mantle. *Geology*, *28*(6), 507–510. https://doi.org/10.1130/0091-7613(2000)28<507:LIEFLE>2.0.CO;2

Tomascak, P. B., Tera, F., Helz, R. T., & Walker, R. J. (1999). The absence of lithium isotope fractionation during basalt differentiation: New measurements by multicollector sector ICP-MS. *Geochimica et Cosmochimica Acta*, *63*(6), 907–910. https://doi.org/10.1016/S0016-7037(98)00318-4

Tomascak, P. B., Widom, E., Benton, L. D., Goldstein, S. L., & Ryan, J. G. (2002). The control of lithium budgets in island arcs. *Earth and Planetary Science Letters*, *196*(3), 227–238. https://doi.org/10.1016/S0012-821X(01)00614-8

Ulmer, P., & Trommsdorff, V. (1995). Serpentine stability to mantle depths and subduction-related magmatism. *Science*, *268*(5212), 858–861. https://doi.org/10.1126/science.268.5212.85

van Keken, P. E., Hacker, B. R., Syracuse, E. M., & Abers, G. A. (2011). Subduction factory: 4. Depth-dependent flux of H_2O from subducting slabs worldwide. *Journal of Geophysical Research*, *116*(B1), B01401. https://doi.org/10.1029/2010JB007922

Vigier, N., Decarreau, A., Millot, R., Carignan, J., Petit, S., & France-Lanord, C. (2008). Quantifying Li isotope fractionation during smectite formation and implications for the Li cycle. *Geochimica et Cosmochimica Acta*, *72*(3), 780–792. https://doi.org/10.1016/S0016-7037(98)00318-4

Vils, F., Pelletier, L., Kalt, A., Müntener, O., & Ludwig, T. (2008). The lithium, boron and beryllium content of serpentinized peridotites from ODP Leg 209 (Sites 1272A and 1274A): Implications for lithium and boron budgets of oceanic lithosphere. *Geochimica et Cosmochimica Acta*, *72*(22), 5475–5504. https://doi.org/10.1016/j.gca.2008.08.005

Vils, F., Tonarini, S., Kalt, A., & Seitz, H. M. (2009). Boron, lithium and strontium isotopes as tracers of seawater–serpentinite interaction at Mid-Atlantic Ridge, ODP Leg 209. *Earth and Planetary Science Letters*, *286*(3–4), 414–425. https://doi.org/10.1016/j.epsl.2009.07.005

Wada, I., & Wang, K. (2009). Common depth of slab-mantle decoupling: Reconciling diversity and uniformity of subduction zones. *Geochemistry, Geophysics, Geosystems*, *10*(10), Q10009. https://doi.org/10.1029/2009GC002570

Walker, J. A., Teipel, A. P., Ryan, J. G., & Syracuse, E. (2009). Light elements and Li isotopes across the northern portion of the Central American subduction zone. *Geochemistry, Geophysics, Geosystems*, *10*(6), Q06S16. https://doi.org/10.1029/2009GC002414

Walowski, K. J., Wallace, P. J., Clynne, M. A., Rasmussen, D. J., & Weis, D. (2016). Slab melting and magma formation beneath the southern Cascade arc. *Earth and Planetary Science Letters*, *446*, 100–112. https://doi.org/10.1016/j.epsl.2016.03.044

Walowski, K. J., Wallace, P. J., Hauri, E. H., Wada, I., & Clynne, M. A. (2015). Slab melting beneath the Cascade arc driven by dehydration of altered oceanic peridotite. *Nature Geoscience*, *8*(5), 404–408. https://doi.org/10.1038/ngeo2417

Webster, J. D., Holloway, J. R., & Hervig, R. L. (1989). Partitioning of lithophile trace elements between H_2O and $H_2O + CO_2$ fluids and topaz rhyolite melt. *Economic Geology*, *84*(1), 116–134. https://doi.org/10.2113/gsecongeo.84.1.116

Weyer, S., & Seitz, H. (2012). Coupled lithium- and iron isotope fractionation during magmatic differentiation. *Chemical Geology*, *294*, 42–50. https://doi.org/10.1016/j.chemgeo.2011.11.020

Wunder, B., Meixner, A., Romer, R. L., & Heinrich, W. (2006). Temperature-dependent isotopic fractionation of lithium between clinopyroxene and high-pressure hydrous fluids. *Contributions to Mineralogy and Petrology*, *151*(1), 112–120. https://doi.org/10.1007/s00410-005-0049-0

Yamane, N., Kanagawa, K., & Ito, T. (2012). Contrasting seismic reflectivity of the lower crust and uppermost mantle between NE Japan and SW Japan as illustrated by petrophysical analyses of mafic and ultramafic xenoliths. *Journal of Geophysical Research*, *117*(B9), B09203. https://doi.org/10.1029/2011JB009008

Yogodzinski, G. M., Brown, S. T., Kelemen, P. B., Vervoort, J. D., Portnyagin, M., Sims, K. W., et al. (2015). The role of subducted basalt in the source of island arc magmas: Evidence from seafloor lavas of the western Aleutians. *Journal of Petrology*, *56*(3), 441–492. https://doi.org/10.1093/petrology/egv006

Yokoyama, T., Kobayashi, K., Kuritani, T., & Nakamura, E. (2003). Mantle metasomatism and rapid ascent of slab components beneath island arcs: Evidence from ^{238}U-^{230}Th-^{226}Ra disequilibria of Miyakejima volcano, Izu arc, Japan. *Journal of Geophysical Research*, *108*(B7), 2329. https://doi.org/10.1029/2002JB002103

You, C. F., Chan, L. H., Spivack, A. J., & Gieskes, J. M. (1995). Lithium, boron, and their isotopes in sediments and pore waters of Ocean Drilling Program Site 808, Nankai Trough; implications for fluid expulsion in accretionary prisms. *Geology*, *23*(1), 37–40. https://doi.org/10.1130/0091-7613(1995)023<0037:LBATII>2.3.CO;2

Zack, T., Tomascak, P. B., Rudnick, R. L., Dalpé, C., & McDonough, W. F. (2003). Extremely light Li in orogenic eclogites: The role of isotope fractionation during dehydration in subducted oceanic crust. *Earth and Planetary Science Letters*, *208*(3–4), 279–290. https://doi.org/10.1016/S0012-821X(03)00035-9

Zeng, Z., Li, X., Zhang, Y., & Qi, H. (2021). Lithium, oxygen and magnesium isotope systematics of volcanic rocks in the Okinawa Trough: Implications for plate subduction studies. *Journal of Marine Science and Engineering*, *10*(1), 40. https://doi.org/10.3390/jmse10010040

Zhang, W., Tanaka, R., Kitagawa, H., Bohlin, M., & Nakamura, E. (2022). A rapid method of simultaneous chromatographic purification of Li and Mg for isotopic analyses using MC-ICP-MS. *International Journal of Mass Spectrometry*, *480*, 116893. https://doi.org/10.1016/j.ijms.2022.116893

Zhao, D., Yanada, T., Hasegawa, A., Umino, N., & Wei, W. (2012). Imaging the subducting slabs and mantle upwelling under the Japan Islands. *Geophysical Journal International*, *190*(2), 816–828. https://doi.org/10.1111/j.1365-246X.2012.05550.x

References From the Supporting Information

Akizawa, N., Ohara, Y., Okino, K., Ishizuka, O., Yamashita, H., Machida, S., et al. (2021). Geochemical characteristics of back-arc basin lower crust and upper mantle at final spreading stage of Shikoku Basin: An example of Mado Megamullion. *Progress in Earth and Planetary Science*, *8*(1), 1–24. https://doi.org/10.1186/s40645-021-00454-3

Begemann, F., Ludwig, K. R., Lugmair, G. W., Min, K., Nyquist, L. E., Patchett, P. J., et al. (2001). Call for an improved set of decay constants for geochronological use. *Geochimica et Cosmochimica Acta*, *65*(1), 111–121. https://doi.org/10.1016/S0016-7037(00)00512-3

Blichert-Toft, J., & Albarede, F. (1997). The Lu-Hf isotope geochemistry of chondrites and the evolution of the mantle-crust system. *Earth and Planetary Science Letters*, *148*(1–2), 243–258. https://doi.org/10.1016/S0012-821X(97)00040-X

Bouvier, A., Vervoort, J. D., & Patchett, P. J. (2008). The Lu–Hf and Sm–Nd isotopic composition of CHUR: Constraints from unequilibrated chondrites and implications for the bulk composition of terrestrial planets. *Earth and Planetary Science Letters*, *273*(1–2), 48–57. https://doi.org/10.1016/j.epsl.2008.06.010

Chan, L. H., Edmond, J. M., & Thompson, G. (1993). A lithium isotope study of hot springs and metabasalts from mid-ocean ridge hydrothermal systems. *Journal of Geophysical Research*, *98*(B6), 9653–9659. https://doi.org/10.1029/92JB00840

Chan, L. H., Edmond, J. M., Thompson, G., & Gillis, K. (1992). Lithium isotopic composition of submarine basalts: Implications for the lithium cycle in the oceans. *Earth and Planetary Science Letters*, *108*(1–3), 151–160. https://doi.org/10.1016/0012-821X(92)90067-6

Chen, S., Hou, T., Liu, J., & Zhang, Z. (2020). Geochemical variation of Miocene Basalts within Shikoku Basin: Magma source compositions and geodynamic implications. *Minerals*, *11*(1), 25. https://doi.org/10.3390/min11010025

Connolly, J. A. (2005). Computation of phase equilibria by linear programming: A tool for geodynamic modeling and its application to subduction zone decarbonation. *Earth and Planetary Science Letters*, *236*(1–2), 524–541. https://doi.org/10.1016/j.epsl.2005.04.033

Decitre, S., Buatier, M., & James, R. (2004). Li and Li isotopic composition of hydrothermally altered sediments at Middle Valley, Juan De Fuca. *Chemical Geology*, *211*(3–4), 363–373. https://doi.org/10.1016/j.chemgeo.2004.07.005

Dunn, T., & Sen, C. (1994). Mineral/matrix partition coefficients for orthopyroxene, plagioclase, and olivine in basaltic to andesitic systems: A combined analytical and experimental study. *Geochimica et Cosmochimica Acta*, *58*(2), 717–733. https://doi.org/10.1016/0016-7037(94)90501-0

Holycross, M. E., Watson, E. B., Richter, F. M., & Villeneuve, J. (2018). Diffusive fractionation of Li isotopes in wet, highly silicic melts. *Geochemical Perspectives Letters*, *6*, 39–42. https://doi.org/10.7185/geochemlet.1807

Klemme, S., Blundy, J. D., & Wood, B. J. (2002). Experimental constraints on major and trace element partitioning during partial melting of eclogite. *Geochimica et Cosmochimica Acta*, *66*(17), 3109–3123. https://doi.org/10.1016/S0016-7037(02)00859-1

Lu, Y., Makishima, A., & Nakamura, E. (2007a). Purification of Hf in silicate materials using extraction chromatographic resin, and its application to precise determination of 176Hf/177Hf by MC-ICP-MS with 179Hf spike. *Journal of Analytical Atomic Spectrometry*, *22*(1), 69–76. https://doi.org/10.1039/B610197F

Lu, Y., Makishima, A., & Nakamura, E. (2007b). Coprecipitation of Ti, Mo, Sn and Sb with fluorides and application to determination of B, Ti, Zr, Nb, Mo, Sn, Sb, Hf and Ta by ICP-MS. *Chemical Geology*, *236*(1–2), 13–26. https://doi.org/10.1016/j.chemgeo.2006.08.007

Makishima, A., & Nakamura, E. (2006). Determination of major/minor and trace elements in silicate samples by ICP-QMS and ICP-SFMS applying isotope dilution-internal standardisation (ID-IS) and multi-stage internal standardisation. *Geostandards and Geoanalytical Research*, *30*(3), 245–271. https://doi.org/10.1111/j.1751-908X.2006.tb01066.x

Makishima, A., Nath, B. N., & Nakamura, E. (2008). New sequential separation procedure for Sr, Nd and Pb isotope ratio measurement in geological material using MC-ICP-MS and TIMS. *Geochemical Journal*, *42*(3), 237–246. https://doi.org/10.2343/geochemj.42.237

Marschall, H. R., Altherr, R., & Rupke, L. (2007). Squeezing out the slab — Modelling the release of Li, Be and B during progressive high-pressure metamorphism. *Chemical Geology*, *239*(3–4), 323–335. https://doi.org/10.1016/j.chemgeo.2006.08.008

Marschall, H. R., Altherr, R., Ludwig, T., Kalt, A., Gmeling, K., & Kasztovszky, Z. (2006). Partitioning and budget of Li, Be and B in high-pressure metamorphic rocks. *Geochimica et Cosmochimica Acta*, *70*(18), 4750–4769. https://doi.org/10.1016/j.gca.2006.07.006

Marsh, B. D. (1979). Island arc development: Some observations, experiments, and speculations. *The Journal of Geology*, *87*(6), 687–713. https://doi.org/10.1086/628460

Nebel, O., Vroon, P. Z., van Westrenen, W., Iizuka, T., & Davies, G. R. (2011). The effect of sediment recycling in subduction zones on the Hf isotope character of new arc crust, Banda arc, Indonesia. *Earth and Planetary Science Letters*, *303*(3–4), 240–250. https://doi.org/10.1016/j.epsl.2010.12.053

Okino, K., Shimakawa, Y., & Nagaoka, S. (1994). Evolution of the Shikoku basin. *Journal of Geomagnetism and Geoelectricity*, *46*(6), 463–479. https://doi.org/10.5636/jgg.46.463

Richter, F. M., Liang, Y., & Davis, A. M. (1999). Isotope fractionation by diffusion in molten oxides. *Geochimica et Cosmochimica Acta*, *63*(18), 2853–2861. https://doi.org/10.1016/S0016-7037(99)00164-7

Schmidt, M. W., & Poli, S. (2003). Generation of mobile components during subduction of oceanic crust. *Treatise on Geochemistry*, *3*, 659–591. https://doi.org/10.1016/B0-08-043751-6/03034-6

Shaw, D. M. (1970). Trace element fractionation during anatexis. *Geochimica et Cosmochimica Acta*, *34*(2), 237–243. https://doi.org/10.1016/0016-7037(70)90009-8

Soderlund, U., Patchett, P. J., Vervoort, J. D., & Isachsen, C. E. (2004). The 176Lu decay constant determined by Lu–Hf and U–Pb isotope systematics of Precambrian mafic intrusions. *Earth and Planetary Science Letters*, *219*(3), 311–324. https://doi.org/10.1016/S0012-821X(04)00012-3

Spallanzani, R., Koga, K. T., Cichy, S. B., Wiedenbeck, M., Schmidt, B. C., Oelze, M., & Wilke, M. (2022). Lithium and boron diffusivity and isotopic fractionation in hydrated rhyolitic melts. *Contributions to Mineralogy and Petrology*, *177*(8), 1–17. https://doi.org/10.1007/s00410-022-01937-2

Steiger, R. H., & Jager, E. (1977). Subcommission on geochronology: Convention on the use of decay constants in geo-and cosmochronology. *Earth and Planetary Science Letters*, *36*(3), 359–362. https://doi.org/10.1016/0012-821X(77)90060-7

Tatsumi, Y., Ishikawa, N., Anno, K., Ishizaka, K., & Itaya, T. (2001). Tectonic setting of high-Mg andesite magmatism in the SW Japan arc: K–Ar chronology of the Setouchi volcanic belt. *Geophysical Journal International*, *144*(3), 625–631. https://doi.org/10.1046/j.1365-246x.2001.01358.x

Uchiumi, S., Uto, K., & Shibata, K. (1989). K-Ar ages of rock reference materials. *Journal of the Mass Spectrometry Society of Japan*, *37*(6), 375–381. https://doi.org/10.5702/massspec.37.375

Vervoort, J. D., & Blichert-Toft, J. (1999). Evolution of the depleted mantle: Hf isotope evidence from juvenile rocks through time. *Geochimica et Cosmochimica Acta*, *63*(3–4), 533–556. https://doi.org/10.1016/S0016-7037(98)00274-9

Wunder, B., Meixner, A., Romer, R. L., Feenstra, A., Schettler, G., & Heinrich, W. (2007). Lithium isotope fractionation between Li-bearing staurolite, Li-mica and aqueous fluids: An experimental study. *Chemical Geology*, *238*(3–4), 277–290. https://doi.org/10.1016/j.chemgeo.2006.12.001

Yamamoto, K., Nakamaru, K., & Adachi, M. (1997). Depositional environments of "accreted bedded cherts" in the Shimanto terrane, Southwest Japan, on the basis of major and minor element compositions. *The Journal of Earth and Planetary Sciences*, *44*, 1–19. https://doi.org/10.1016/0037-0738(87)90017-0

Yokoyama, T., Makishima, A., & Nakamura, E. (1999). Evaluation of the coprecipitation of incompatible trace elements with fluoride during silicate rock dissolution by acid digestion. *Chemical Geology*, *157*(3), 175–187. https://doi.org/10.1016/S0009-2541(98)00206-X

Yoshikawa, M., & Nakamura, E. (1993). Precise isotope determination of trace amounts of Sr in magnesium-rich samples. *Journal of Mineralogy, Petrology and Economic Geology*, *88*(12), 548–561. https://doi.org/10.2465/ganko.88.548